การสังเคราะห์คอมพอสิตแคลเซียมฟอสเฟตที่มีสมบัติแม่เหล็กโดยใช้กรดซิตริกเป็นสารเติมแต่ง
สำหรับการขจัดแคดเมียมจากสารละลายน้ำ

นางสาวตรัง ทุย ทุย เลอ ฮวง



วิทยานิพนธ์นี้เป็นส่วนหนึ่งของการศึกษาตามหลักสูตรปริญญาวิทยาศาสตรมหาบัณฑิต
สาขาวิชาเคมี ภาควิชาเคมี
คณะวิทยาศาสตร์ จุฬาลงกรณ์มหาวิทยาลัย
ปีการศึกษา 2559

# SYNTHESIS OF MAGNETIC CALCIUM PHOSPHATE COMPOSITES USING CITRIC ACID AS ADDITIVE FOR REMOVAL OF CADMIUM FROM AQUEOUS SOLUTION

Miss Trang Thuy Thuy Le Hoang


A Thesis Submitted in Partial Fulfillment of the Requirements
for the Degree of Master of Science Program in Chemistry
Department of Chemistry
Faculty of Science
Chulalongkorn University
Academic Year 2016

| | |
|---|---|
| Thesis Title | SYNTHESIS OF MAGNETIC CALCIUM PHOSPHATE COMPOSITES USING CITRIC ACID AS ADDITIVE FOR REMOVAL OF CADMIUM FROM AQUEOUS SOLUTION |
| By | Miss Trang Thuy Thuy Le Hoang |
| Field of Study | Chemistry |
| Thesis Advisor | Nipaka Sukpirom, Ph.D. |
| Thesis Co-Advisor | Assistant Professor Fuangfa Unob, Ph.D. |

Accepted by the Faculty of Science, Chulalongkorn University in Partial Fulfillment of the Requirements for the Master's Degree

.....Dean of the Faculty of Science
(Associate Professor Polkit Sangvanich, Ph.D.)

THESIS COMMITTEE

.....Chairman
(Associate Professor Vudhichai Parasuk, Ph.D.)

.....Thesis Advisor
(Nipaka Sukpirom, Ph.D.)

.....Thesis Co-Advisor
(Assistant Professor Fuangfa Unob, Ph.D.)

.....Examiner
(Numpon Insin, Ph.D.)

.....External Examiner
(Assistant Professor Jinda Yeyongchaiwat, Ph.D.)

ตรัง ทุย ทุย เลอ ฮวง : การสังเคราะห์คอมพอสิตแคลเซียมฟอสเฟตที่มีสมบัติแม่เหล็กโดยใช้กรดซิตริกเป็นสารเติมแต่งสำหรับการขจัดแคดเมียมจากสารละลายน้ำ (SYNTHESIS OF MAGNETIC CALCIUM PHOSPHATE COMPOSITES USING CITRIC ACID AS ADDITIVE FOR REMOVAL OF CADMIUM FROM AQUEOUS SOLUTION) อ.ที่ปรึกษาวิทยานิพนธ์หลัก: ดร. นิปกา สุขภิรมย์, อ.ที่ปรึกษาวิทยานิพนธ์ร่วม: ผศ. ดร. เฟื่องฟ้า อุ่นอบ, 61 หน้า.

งานวิจัยนี้ได้สังเคราะห์สารประกอบแคลเซียมฟอสเฟตที่มีสมบัติแม่เหล็กโดยใช้กรดซิตริกเป็นตัวช่วยด้วยกระบวนการสังเคราะห์ขั้นตอนเดียว โดยทั่วไปสารประกอบแคลเซียมฟอสเฟตถูกพบในรูปของสารประกอบไฮดรอกซีอะพาไทต์ (Hap) ในงานนี้พบว่าการสังเคราะห์ในสภาวะที่มี $Fe_3O_4$ และกรดซิตริกอยู่สามารถทำให้เกิดเฟสกึ่งเสถียรของแคลเซียมฟอสเฟตในรูปอสัณฐาน (ACP) ได้ โดย $Fe_3O_4$ อาจทำหน้าที่ป้องกันการรวมตัวกันของนิวคลีไอแคลเซียมฟอสเฟต และกรดซิตริกทำหน้าที่ป้องกันแคลเซียมฟอสเฟตรูปอสัณฐานไม่ให้เปลี่ยนเป็นสารประกอบไฮดรอกซีอะพาไทต์ ซึ่งความสามารถในการป้องกันการเปลี่ยนเฟสนี้จะขึ้นกับรูปของกรดซิตริกในสารละลายด้วย กล่าวคือหากใช้กรดซิตริกในรูป fully-deprotonate จะทำให้เกิดเฟส Hap ขณะที่การใช้สปีชีส์อื่นจะทำให้เกิดเฟส ACP สารประกอบที่สังเคราะห์ได้ถูกพิสูจน์เอกลักษณ์ด้วยเทคนิค XRD, FTIR, elemental analysis, DSC, surface area analyzer, TEM, SEM และ VSM นอกจากนี้ยังพบว่าสารประกอบที่สังเคราะห์ได้สามารถแยกออกจากสารละลายได้ง่ายด้วยแม่เหล็กจากภายนอก

ในสารประกอบที่สังเคราะห์ได้ทั้งหมดนี้ พบว่าสารประกอบ ACP/$Fe_3O_4$/citric ที่มีสัดส่วนของ Ca/P เท่ากับ 1.5 มีความสามารถในการดูดซับแคดเมียมมากที่สุด จากการศึกษาจลนศาสตร์การดูดซับและไอโซเทอมการดูดซับแคดเมียมบนสารประกอบ ACP/$Fe_3O_4$/citric พบว่าโมเดลจลนศาสตร์การดูดซับอันดับสองเทียมและโมเดลไอโซเทอมการดูดซับแบบแลงเมียร์สามารถอธิบายกลไกและพฤติกรรมการดูดซับได้ดี ความสามารถในการดูดซับสูงสุดคำนวณจากโมเดลของแลงเมียร์มีค่าเท่ากับ 270.3 mg $g^{-1}$ และกลไกการดูดซับเกิดจากการแลกเปลี่ยนแคทไอออนระหว่าง $Ca^{2+}$ ในสารประกอบแคลเซียมฟอสเฟตกับ $Cd^{2+}$ ในสารละลาย โดยสารประกอบจะมีความสามารถในการดูดซับแคดเมียมสูงเมื่อสารประกอบที่สังเคราะห์ได้มีความเป็นผลึกต่ำ ความสามารถในการดูดซับแคดเมียมมีค่าเพิ่มขึ้นเมื่อเพิ่ม pH จาก 2 เป็น 3 และมีค่าคงที่ในช่วง pH 3 ถึง 7

| | |
|---|---|
| ภาควิชา เคมี | ลายมือชื่อนิสิต ..... |
| สาขาวิชา เคมี | ลายมือชื่อ อ.ที่ปรึกษาหลัก ..... |
| ปีการศึกษา 2559 | ลายมือชื่อ อ.ที่ปรึกษาร่วม ..... |

# # 5772276823 : MAJOR CHEMISTRY

KEYWORDS: CALCIUM PHOSPHATE / CADMIUM REMOVAL / CITRIC ACID / MAGNETITE

TRANG THUY THUY LE HOANG: SYNTHESIS OF MAGNETIC CALCIUM PHOSPHATE COMPOSITES USING CITRIC ACID AS ADDITIVE FOR REMOVAL OF CADMIUM FROM AQUEOUS SOLUTION. ADVISOR: NIPAKA SUKPIROM, Ph.D., CO-ADVISOR: ASST. PROF. FUANGFA UNOB, Ph.D., 61 pp.

Magnetic calcium phosphate composites were successfully synthesized in the presence of citric acid via one-pot synthesis. The phase of calcium phosphates was normally found as hydroxyapatite phase (Hap). However, the metastable phase of amorphous calcium phosphate (ACP) could occur in the presence of preformed $Fe_3O_4$ particles and citric acid. $Fe_3O_4$ might prevent the aggregation of calcium phosphate nuclei, and citric acid was found to inhibit the transformation of ACP into Hap. The inhibiting ability of citric acid depended strongly on the species of citric acid in the solution. The fully-deprotonate form promoted Hap, while the less deprotonated species yielded ACP. The materials were characterized by XRD, FTIR, elemental analysis, DSC, surface area analyzer, TEM, SEM, and VSM. Under external magnetic field, the used adsorbents were removed easily from aqueous solution showing high potential for convenient separation.

Among the prepared magnetic calcium phosphate composites, the ACP/$Fe_3O_4$/citric sample having Ca/P ratio of 1.5 shown the highest cadmium capacity. The adsorption isotherm and kinetics of this adsorbent were fitted with Langmuir model and pseudo-second-order model, respectively. The maximum adsorption capacity achieved from the Langmuir model was 270.3 mg $g^{-1}$. The sorption mechanism was found to be cation exchange between $Ca^{2+}$ in calcium phosphate materials and $Cd^{2+}$ in the solution. Higher cadmium capacity was achieved from the materials having lower crystallinities. The cadmium adsorption capacity increased when the initial pH of the $Cd^{2+}$ solution increased from 2 to 3, and remained constant between pH of 3 to 7.



| | | |
|---|---|---|
| Department: | Chemistry | Student's Signature ..... |
| Field of Study: | Chemistry | Advisor's Signature ..... |
| Academic Year: | 2016 | Co-Advisor's Signature ..... |

# ACKNOWLEDGEMENTS

The author wishes to express her sincere appreciation to Dr. Nipaka Sukpirom, her advisor and Assistant Professor Dr. Fuangfa Unob, her co-advisor for their guidance, support and encouragement throughout this research. She would like to extend her appreciation to Associate Professor Dr. Vudhichai Parasuk, Dr. Numpon Insin, Assistant Professor Dr. Apichat Imyim, Assistant Professor Dr. Kanet Wongravee, and Assistant Professor Dr. Jinda Yeyongchaiwat for their valuable suggestions.

The author would like to thank the H.M. the King Bhumibhol Adulyadej's 72nd Birthday Anniversary Scholarship for the financial supports. She is really grateful for all kind support and opportunities that this award provided her for achieving her educational goals.

She also wishes to acknowledge Dr. Soonthorn Suvokhiaw, her friends and all members of Materials Chemistry and Catalysis Research Unit and Environmental Analysis Research Unit for their kind suggestion and encouragement.

Finally, the author would like to express her deepest gratitude to her family in Vietnam for their love, trust and support. She is also grateful to her boyfriend for his kind help and encouragement throughout two years she studied abroad.

**CONTENTS**

Page

Page

Page

## LIST OF FIGURES

# LIST OF TABLES

# CHAPTER 1
# INTRODUCTION

## 1.1 Characteristics and toxicity of cadmium

Cadmium is a chemical element residing in 12$^{th}$ group of the periodic table with an atomic number of 48. It mainly occurs with oxidation state +2 as a byproduct in Zinc and Lead ores [1]. In aqueous solution, the distribution of different cadmium (II) species, including $Cd^{2+}$, $Cd(OH)^{+}$, $Cd(OH)_2$ and $Cd(OH)^{3-}$ depends on the pH of the solution and the concentration of cadmium. With the pH lower than 6, $Cd^{2+}$ is the only species found in the solution (Figure 1.1) [2].

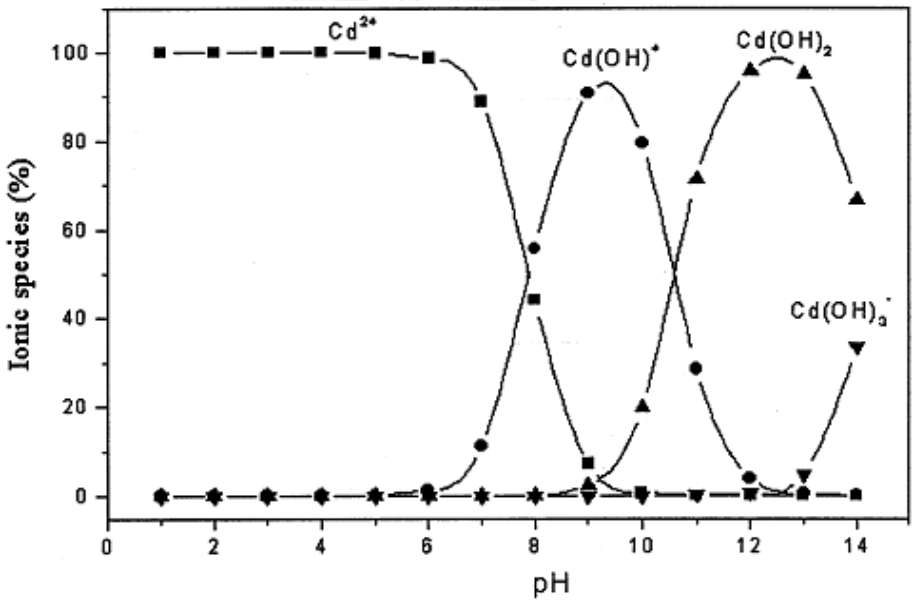


Figure 1.1 Various types of hydrolyzed $Cd^{2+}$ at different pH [2]

Cadmium has various uses in industry. It could be used in manufacturing of Ni-Cd batteries, electroplating, industry paints, or nuclear fission. However, this element is classified as one of extremely toxic heavy metals. Cadmium is well-known for causing kidney disease, bone defects, and lung cancer. At present, the high level of cadmium leaked from both natural and anthropogenic sources contaminates the environment, especially the water resources. Therefore, numerous processes for removal of cadmium from aqueous solution, such as precipitation, flotation, ion exchange,

adsorption, and membrane filtration, have been widely investigated. Although choosing an appropriate method depends on the specific purposes and conditions of each process, applying low-cost, non-toxic and effective materials is preferred [3].

## 1.2 Calcium phosphate (CPs) materials

Calcium phosphates (CPs) materials have received a lot of attention in the field of waste treatment [4-15]. CPs have many advantages, such as availability, low water solubility, non-toxicity, low cost, and high ability for metals uptake. Two types of CPs, including hydroxyapatite-based materials [5-10, 13-15] and amorphous calcium phosphate [4] have been known for their potential applications in the removal of heavy metals, especially cadmium.

### 1.2.1 Hydroxyapatite and its application for cadmium removal

Hydroxyapatite (Hap) ($Ca_{10}(PO_4)_6(OH)_2$) is one type of apatite minerals occurring naturally in the world. It is also known as a major component of bones and teeth. Hap has a hexagonal crystal structure. Its smallest building unit projected down [001] direction was represented in Figure 1.2 [16].

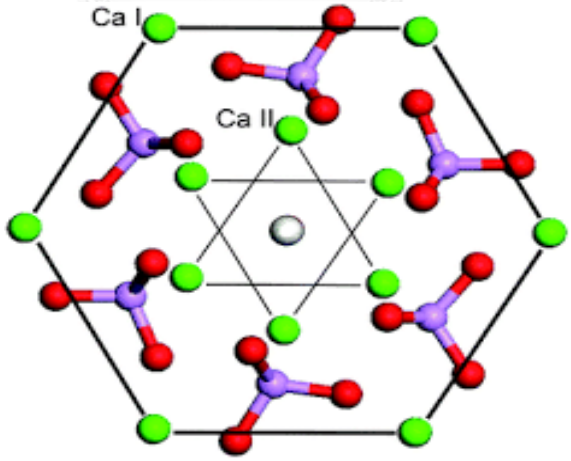


Figure 1.2 Structure of hydroxyapatite (phosphorous: purple, oxygen: red, calcium: green, hydroxyl-: white) [16]

Hap has been extensively studied for removing heavy metals [2, 5, 6, 8-10, 17, 18], especially for $Cd^{2+}$ removal [3, 5-7, 9, 19] – the application studied in this work. These researchers reported that the removal of $Cd^{2+}$ by Hap reaching relatively high

maximum capacities, in the range of 66.55 – 260.42 mg $g^{-1}$. Hap was found to have higher maximum capacities than many sorbents, such as treated clay (24.45 mg $g^{-1}$) [20], treated rice husk (29.54 mg $g^{-1}$) [20], or chitosan/activated carbon (52.63 mg $g^{-1}$) [21]. The mechanism of the removal process was studied, and there were a good agreements that $Cd^{2+}$ entered Hap by ion exchange with $Ca^{2+}$ [6, 14, 15, 17]. In details, $Cd^{2+}$ firstly formed a complexation on ≡POH site of Hap surface (HA–OH + $Cd^{2+}$ → HA–O–$Cd^{+}$ + $H^{+}$). Then $Cd^{2+}$ would be exchanged with $Ca^{2+}$ to form a Cd-containing Hap, $Cd_xCa_{10-x}(PO_4)_6(OH)_2$ (HA–$Ca^{2+}$ + $Cd^{2+}$ → HA–$Cd^{2+}$ + $Ca^{2+}$). The adsorption isotherms and kinetics were also studied and considered to be fitted with Langmuir model [6, 9] and pseudo-second order [17], respectively. These results might indicate the chemisorption between Hap surface and $Cd^{2+}$ in the solution.

Hap has been synthesized by many methods, such as sol-gel approach, hydrothermal method, precipitation, multiple emulsion technique, or biomimetic deposition technique [22]. Among them, precipitation technique is the most popular technique because the procedure is cheap, simple and fast. The examples of precipitation reactions were shown below [22]:

$$10\ Ca(OH)_2 + 6H_3PO_4 \longrightarrow Ca_{10}(PO_4)_6(OH)_2 + 18\ H_2O$$

$$10\ Ca(OH)_2 + 6\ (NH_4)_2.HPO_4 \longrightarrow Ca_{10}(PO_4)_6(OH)_2 + 6\ H_2O + 12\ NH_4OH$$

$$7\ Ca(OH)_2 + 3\ Ca(H_2PO_4)_2.H_2O \longrightarrow Ca_{10}(PO_4)_6(OH)_2 + 15\ H_2O$$

$$Ca(EDTA)_2^{-} + 3/5\ HPO_4^{2-} + 2/5\ H_2O \longrightarrow 1/10\ Ca_{10}(PO_4)_6(OH)_2 + HEDTA^{3-} + 1/5\ OH^{-}$$

**1.2.2 Amorphous calcium phosphate and its application for cadmium removal**

ACP is a meta-stable species, formed as a precursor of Hap in a basic condition. From a saturated calcium phosphates solution, ACP precipitates as an initial solid phase, then readily transform to the stable crystalline materials, Hap [23-25]. Therefore, to synthesize ACP, adding additive, using special starting materials or freeze-drying were necessary in order to prevent the transformation from ACP to crystalline CPs phases. Up to date, there are three methods have been used for ACP synthesis, including microwave-assisted hydrothermal, precipitation and spray drying method [4, 26-28]. In microwave-assisted hydrothermal method, phosphorus-containing

biomolecules, such as β-glycerophosphate disodium and adenosine triphosphate were used as phosphate sources. These phosphorus-containing biomolecules could release phosphate from the hydrolysis process by heat treatment to control the calcium phosphates growth. With precipitation method, ACP was achieved from the reaction between calcium and phosphate salts in basic solution followed by a freeze-drying, calcination and storage at very low temperature (-18°C) to avoid the transformation from ACP to Hap.

ACP has various Ca/P ratio (~ 1.0 - 2.0) depending on the condition of the synthesis [27, 29, 30]. In basic condition (pH 9-11), amorphous tricalcium phosphate ($Ca_3(PO_4)_2.nH_2O$) is most widely achieved. The structure of this compound called "Posner's clusters" was shown in Figure 1.3. In acidic condition, the ratio of 1.15 was obtained. Moreover, Ca/P ratio much lower than 1.5 corresponding to amorphous OCP [$Ca_8H_2(PO_4)_4.nH_2O$] or amorphous DCP ($CaHPO_4$) could be achieved in non - aqueous solution. For the ratio higher than 1.5, the foreign ions, such as carbonate or oxide ions, are needed in the preparation.

ACP precipitates normally contain a large amount of water, including bound water (10-20%) and water molecules in the space between the calcium phosphates clusters. The specific surface area of ACP was therefore surprising low due to the obstruction of these water molecules [27].

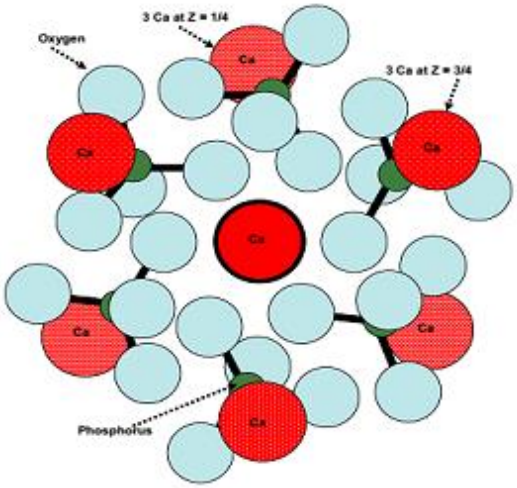


Figure 1.3 Structure of amorphous tricalcium phosphate called “Posner’s clusters” [27]

For heavy removal application, Guan-Jun D. *et al*. synthesized ACP by microwave - assisted hydrothermal and obtained high cadmium removal capacity (366 mg $g^{-1}$) [4]. Moreover, it has been found that higher removal capacities of heavy metals were achieved from hydroxyapatite (Hap) with lower crystallinity and higher specific surface area [31]. Considered the effect of crystalllinity, ACP might be more promising sorbents than Hap [4]. However, up to date, ACP has been less studied than Hap. One of the reasons could be its complicated preparation. Therefore, ACP could catch more interest if the synthesis process is simpler.



**1.3 Synthesis of magnetic CPs composites for the convenient recovery**

Using CPs composites to remove heavy metals normally faces with separation difficulty [13, 32, 33]. A development of convenient recovery is therefore needed. The magnetic separation is well known as an efficient, economic, and no-contaminated technology. The magnetic composites of various sorbents and $Fe_3O_4$ were reported on their easy separation using an external magnetic field [13, 32-35].

For Hap, various Hap/$Fe_3O_4$ composites for heavy metals removal have been synthesized. Feng *et. al*. [13] successfully synthesized magnetic Hap nanoparticles by one-pot co-precipitation method. The prepared materials gave high removal $Cd^{2+}$ capacity of 223.9 (mg $g^{-1}$) and shown the saturation magnetization of 59.4 (emu $g^{-1}$). In

this research, the mechanism of adsorption process was proposed as cationic exchange between $Cd^{2+}$ and Hap/$Fe_3O_4$ surface, which agreed well with many researches using pure Hap mentioned earlier. Kazeminezhad *et al*. [36] successfully prepared Hap/$Fe_3O_4$ nanoparticles by co-precipitation method. The $Cd^{2+}$ removal capacity of the composite was 84.746 (mg $g^{-1}$). The nanoparticles had an average size of 19 ± 2 nm and shown superparamagnetic behavior. Other magnetic Hap/$Fe_3O_4$ composites were also used for other heavy metals removal [32, 33]. Yang *et al*. [33] prepared a core-shell structure using co-precipitation method. Indeed, $Fe_3O_4$ was formed as cores and coated by Hap particles on its surface.

For ACP, due to the complicated synthesis processes, there were only a few researches on magnetic ACP composites and most of them focused on the biochemistry application [37].

### 1.4 Citric acid and its effects to magnetite particles and calcium phosphate materials

In relation to the factors affecting the $Cd^{2+}$ removal efficiency, the particle size and specific surface area are important characteristics of adsorbents. Adding inhibitors or stabilizers are sometimes needed to control the size of particles [14]. Citric acid, a tricarboxylic acid (Figure 1.4), is known as a strong chelating ability to calcium ions. Therefore, it was used as to inhibit the Hap growth [38-40] and the transformation of ACP to Hap [24]. Moreover, citric acid was also used to stabilize the magnetite particles, especially nanoparticles [41-43].

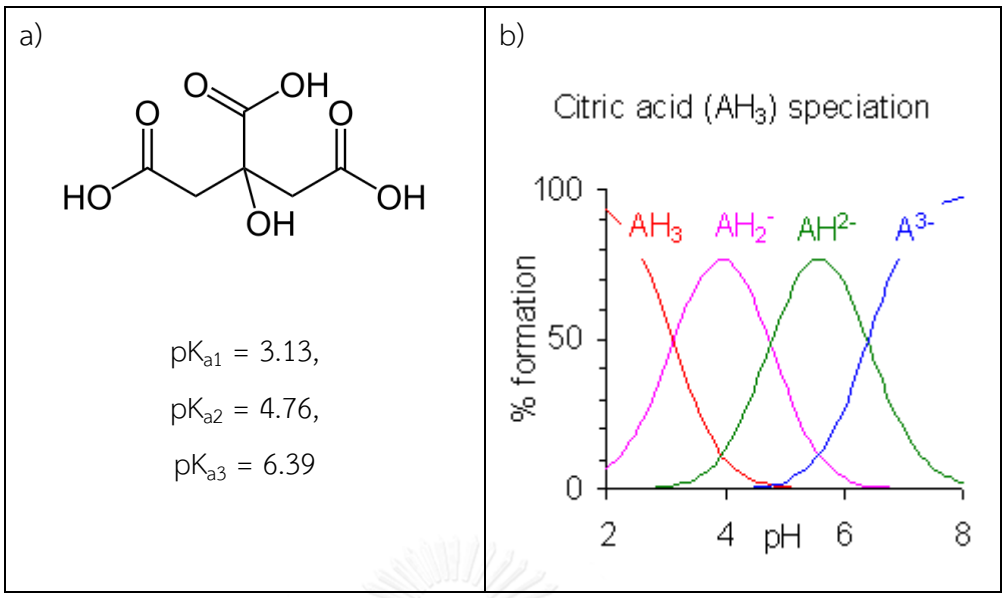


Figure 1.4 Structure of citric acid (a) and its speciation (b)

### 1.4.1 Effect of citric acid to magnetite particles

The application of citric acid as a steric stabilizer coating on magnetite surface was studied. It used one carboxylic group to bind with magnetite surface leaving two carboxyl groups with negative charges to prevent the aggregation or to provide the active sites for further surface modification [41, 42]. Sousa *et al*. [41] prepared citric acid coated magnetite nanoparticles using co-precipitation method for magnetic hyperthermia. They achieved the stable suspension with the highest content of magnetite nanoparticles at the coating pH of 4.58. The coated magnetite had superparamagnetic behavior having magnetite nanoparticle size of 9 - 12 nm. Cheraghipour *et al*. [42] reported similar findings when synthesizing citric-capped superparamagnetic magnetite nanoparticles with the average size of 10 nm, narrow size distribution, and saturation magnetization of 74 (emu $g^{-1}$).

### 1.4.2 Effect of citric acid to calcium phosphate materials

Citric acid and its anionic forms have a strong chelating ability to calcium ions that strongly depended on the pH of the solution [44-46]. The possible associations of different anionic forms of citric acid and free calcium ions [44] were represented in Figure 1.5. The chelating ability of citric acid and calcium ion increases with the increase of negative charge on the species of citric acid in solution.

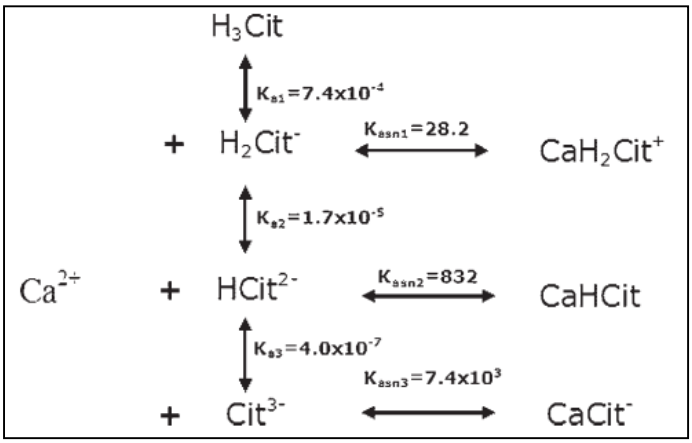


Figure 1.5 Citrate equilibrium and possible associations with free calcium ions [44]

Due to the chelating ability to calcium ion, for Hap, citric acid was used to inhibit and control the particle nucleation and crystal growth [38, 39, 45-47]. Hu *et al*. [45] found that Hap crystal size decreased with increasing citric acid concentration. They proposed that citric acid existed as citrate ions in their condition (pH of 7.5 - 8.0) and it could bind strongly to calcium ions. Therefore, the negative charges were created on Hap surface, which repelled with phosphate ions and other Hap nuclei resulting in the inhibition of further crystal growth and the prevention of particle aggregation. Saoiabi *et. al*. [47] used Hap that was modified with citric acid to remove lead from aqueous solution. They found that citric-modified Hap had faster adsorption rate and higher adsorption capacity than pure Hap. However, most researchers studied the effect of citric acid on Hap only for the biological purpose due to their existence in human bodies. There are few studies in relation to heavy metal removal. For ACP, citric acid was found to be a moderate inhibitor of the transformation of ACP to Hap [24].

## 1.5 The objectives of this study

- To synthesize the magnetic calcium phosphate composites with the assistance of citric acid
- To find out the function of citric acid during the synthesis process as well as the mechanism of this process

- To investigate the cadmium removal ability of the synthesized materials
- To study the adsorption behavior of the composites, and propose the mechanism of the removal process

# CHAPTER 2
# EXPERIMENTAL

## 2.1 Chemicals

All chemicals were listed in Table 2.1.

Table 2. 1 Chemicals used in this work

| Chemicals | Purity (%) | Company |
|---|---|---|
| $Ca(NO_3)_2.4H_2O$ | 90 - 103 | Ajax Finechem |
| $NH_4H_2PO_4$ | 99 | Carbo Erba |
| Citric acid | 99-102 | Ajax Finechem |
| $NH_4OH$ 30% | 28-30 | Carbo Erba |
| $HNO_3$ | 65 | Merck |
| $FeCl_3$ | >97 | Fisher Chemical |
| $FeSO_4.7H_2O$ | 99-104.5 | Loba Chemie |
| $3CdSO_4.8H_2O$ | >99 | Carlo Erba |
| NaOH | >99 | Merck |



## 2.2 Synthesis of Hap, Hap/citric, $Fe_3O_4$, Hap/$Fe_3O_4$, and CPs/$Fe_3O_4$/citric composites

Magnetic calcium phosphate composites were synthesized in the presence of citric acid (CPs/$Fe_3O_4$/citric) via one-pot precipitation method. In order to characterize the nature and evaluate the performance of composite materials, pristine Hap, Hap/citric, bare $Fe_3O_4$ and Hap/$Fe_3O_4$ were also synthesized. ACP could not be synthesized in the synthesis condition of this work because the phase was meta-stable and readily transformed to Hap.

### 2.2.1 Synthesis of $Fe_3O_4$

$Fe_3O_4$ particles were synthesized by modifying the method from the literature [48]. $FeSO_4.7H_2O$ and $FeCl_3$ were dissolved separately and mixed together under nitrogen atmosphere. Concentrated ammonia solution (30%) was added to the mixed solution until the pH of solution reached 10.0. After stirring for 1 hour, the black precipitates were separated by a magnet, centrifuged at 3000 rpm, and washed three times by deionized water. Then, the as-synthesized $Fe_3O_4$ was dried at 60°C under vacuum for 12 hours.

### 2.2.2 Synthesis of Hap

To synthesize Hap, $Ca(NO_3)_2.4H_2O$ and $NH_4H_2PO_4$ (Ca/P molar ratio of 1.67) were dissolved in deionized water and mixed together. Then, concentrated ammonia solution (30%) was added until the pH of the suspension reached 10.5. The reaction occurred as: $10\ Ca(NO_3)_2.4H_2O + 6\ NH_4H_2PO_4 \longrightarrow Ca_{10}(PO_4)_6(OH)_2 + 20\ NH_4NO_3 + 38\ H_2O$. After stirring for 1 hour, the white precipitates were centrifuged at 3000 rpm and washed three times by deionized water. Finally, the received precipitates were dried at 90°C for 12 hours.

### 2.2.3 Synthesis of CPs/$Fe_3O_4$/citric

To synthesize CPs/$Fe_3O_4$/citric composites, $Fe_3O_4$ particles were preformed, using the same method as shown in the section 2.2.1 without collecting or washing the precipitates. Then, the solution of citric acid and starting materials of calcium phosphates were added into the said $Fe_3O_4$ mixture. The mole of citric acid to $Ca^{2+}$ and $Fe^{3+}$ to $Ca^{2+}$ were 0.25:1 and 0.22:1, respectively. The pH of the suspension was adjusted to 10.5 by concentrated ammonia (30%). After stirring for 1 hour, the obtained precipitates were washed two times by deionized water and dried at 90°C.

The optimized condition of the synthesis process, including the order of adding citric acid, $Ca^{2+}$, $PO_4^{3-}$, pH of the reaction mixture and Ca/P ratio were studied and described in Table 2.2

Table 2.2 The conditions of the synthesis process (the variables were shown in **bold text**)

| Parameters | Details |
|---|---|
| The order of adding citric acid, $Ca^{2+}$ and $PO_4^{3-}$ | $Fe_3O_4$ (pH=10) ⟶ **$Ca^{2+}$** ⟶ **Solution of citric** (not control pH) ⟶ **$PO_4^{3-}$** (pH=10.5) Ca/P=1.67 |
| | $Fe_3O_4$ (pH=10) ⟶ **Solution of citric acid** (not control pH) ⟶ **$Ca^{2+}$ + $PO_4^{3-}$** (pH=10.5) Ca/P=1.67 |
| | $Fe_3O_4$ (pH=10) ⟶ **Solution of citric acid + $PO_4^{3-}$** (not control pH) ⟶ **$Ca^{2+}$** (pH=10.5) Ca/P=1.67 |
| | $Fe_3O_4$ (pH=10) ⟶ **Solution of citric acid** (not control pH) ⟶ **$Ca^{2+}$** ⟶ **$PO_4^{3-}$** (pH=10.5) Ca/P=1.67 |
| pH of the reaction mixture after citric acid was added | $Fe_3O_4$ (pH=10) ⟶ Solution of citric acid ⟶ **pH = 2.3** ⟶ $Ca^{2+}$ and $PO_4^{3-}$ (pH=10.5) Ca/P=1.67 |
| | $Fe_3O_4$ (pH=10) ⟶ Solution of citric acid ⟶ **pH = 4.0** ⟶ $Ca^{2+}$ and $PO_4^{3-}$ (pH=10.5) Ca/P=1.67 |
| | $Fe_3O_4$ (pH=10) ⟶ Solution of citric acid ⟶ **pH = 6.0** ⟶ $Ca^{2+}$ and $PO_4^{3-}$ (pH=10.5) Ca/P=1.67 |
| | $Fe_3O_4$ (pH=10) ⟶ Solution of citric acid ⟶ **pH = 6.7** ⟶ $Ca^{2+}$ and $PO_4^{3-}$ (pH=10.5) Ca/P=1.67 |
| | $Fe_3O_4$ (pH=10) ⟶ Solution of citric acid ⟶ **pH = 7.9** ⟶ $Ca^{2+}$ and $PO_4^{3-}$ (pH=10.5) Ca/P=1.67 |
| | $Fe_3O_4$ (pH=10) ⟶ Solution of citric acid ⟶ **pH = 9.5** ⟶ $Ca^{2+}$ and $PO_4^{3-}$ (pH=10.5) Ca/P=1.67 |
| Initial Ca/P ratio | $Fe_3O_4$ (pH=10) ⟶ Solution of citric acid ⟶ pH = 6.0 ⟶ $Ca^{2+}$ and $PO_4^{3-}$ (pH=10.5) **Ca/P =1** |
| | $Fe_3O_4$ (pH=10) ⟶ Solution of citric acid ⟶ pH = 6.0 ⟶ $Ca^{2+}$ and $PO_4^{3-}$ (pH=10.5) **Ca/P =1.5** |
| | $Fe_3O_4$ (pH=10) ⟶ Solution of citric acid ⟶ pH = 6.0 ⟶ $Ca^{2+}$ and $PO_4^{3-}$ (pH=10.5) **Ca/P =1.67** |
| | $Fe_3O_4$ (pH=10) ⟶ Solution of citric acid ⟶ pH = 6.0 ⟶ $Ca^{2+}$ and $PO_4^{3-}$ (pH=10.5) **Ca/P =2** |

### 2.2.4 Synthesis of Hap/$Fe_3O_4$

Hap/$Fe_3O_4$ composites were synthesized in the similar fashion as CPs/$Fe_3O_4$/citric without the presence of citric acid. $Fe_3O_4$ particles were preformed first and follow by adding $Ca^{2+}$ and $PO_4^{3-}$ at the same time. The mole ratio of $Fe^{3+}/Ca^{2+}$ and Ca/P were 0.22 and 1.67, respectively.

### 2.2.5 Synthesis of Hap/citric

Hap/citric was synthesized by following the synthesis procedure of Hap. However, $Ca^{2+}$ and $PO_4^{3-}$ were added at the same time into a solution of citric acid at pH 6.0. The mole of citric acid/$Ca^{2+}$ and Ca/P were 0.25:1 and 1.67, respectively.

## 2.3 Characterization techniques

### 2.3.1 Fourier transform infrared spectroscopy (FTIR)

FTIR was needed to identify the vibrational groups in order to determine the presence of $PO_4^{3-}$, $OH^-$ and citrate ions. The FTIR spectra were recorded as KBr pellets using a Thermo Scientific Nicolet 6700 FTIR spectrophotometer.

### 2.3.2 X-ray powder diffraction (XRD)

To identify the crystalline phases and observe their crystallinities, the Rigaku, Dmax-2200 UltimaPlus X-ray powder diffractometer was used. This instrument was quipped with a monochromater and a Cu Kα radiation source generated at 40 kV and 30 mA. The analysis angles were performed from 2 theta 20° to 70°. The scattering, divergent and receiving slits were set at 1°, 1° and 0.3 mm, respectively.

### 2.3.3 Differential scanning calorimetry (DSC)

In order to understand how citrate ions bonded in the materials, DSC1 Mettler Toledo was used. The measurements were performed by heating samples from 30°C to 450°C in air atmosphere with 10°C $min^{-1}$ heating rate.

### 2.3.4 Elemental analysis

LECO CHNS-628 elemental analyzer at Kasetsart University was used to determine the percentage of carbon element in order to calculate the amount of citrate ions in the final products.

**2.3.5 Transmission electron microscopy (TEM)**

The morphologies and particle sizes of the synthesized materials were determined by using a Philips TECNAI 20 electron microscope at Burapha University. For TEM preparation, the powder samples were dispersed in deionized water (solid/liquid ratio of 1/20 (mg $mL^{-1}$)). The suspensions were sonicated for 20 minutes. Then one drop of the suspensions was placed onto the copper grids. The samples were evaporated naturally and kept at least one week before the determination.

**2.3.6 Scanning electron microscopy (SEM)**

The surface morphology of the materials were monitored by SEM using a JSM-5800 LV scanning electron microscopy (Oxford Instrument Link ISIS series 300) at Faculty of Science, Chulalongkorn University. The samples were prepared by coating onto carbon tabs and drying overnight at 80°C.

**2.3.7 Surface area analysis**

The surface area and pore size distribution of samples were measured by nitrogen adsorption - desorption using BEL Japan BELSORP-mini 28SP instrument. The samples were dried at 90°C overnight. Then they were pretreated at 110°C in the vacuum for 4 hours before the measurements.

**2.3.8. Vibrating sample magnetometer (VSM)**

The magnetic hysteresis loops of composites were recorded using an in - house developed VSM system at Kasetsart University [49]. The system was calibrated by nickel sphere from Lake Shore, model 730908.

**2.4 Adsorption experiments**

Cadmium adsorption process was performed by batch experiments. 10 mg of sorbents was added into a bottle containing 10 mL $Cd^{2+}$. The pH of solution was adjusted to 5.00 by 0.01 M $HNO_3$ and 0.01 M NaOH. Then, the suspensions were shaken at 30 rpm for 24 hours. The samples were collected by using 0.45 micron syringe filters. The concentration of $Cd^{2+}$ was determined by inductively coupled plasma (ICP-OES) model iCAP 6500 series (Thermo Fisher scientific). The cadmium adsorption capacity was calculated by:

$$q_t = [(C_o - C_t)V]/m$$

where $q_e$ (mg $g^{-1}$) is the cadmium removal capacity, $C_o$ and $C_t$ are the $Cd^{2+}$ initial concentration and $Cd^{2+}$ concentration at time *t*, respectively (mg $L^{-1}$). *V* is the volume of solution (L), and *m* is the weight of sorbents (g).

**2.4.1 Effect of contact time**

To study the adsorption kinetics, the contact time was varied from 5 to 420 minutes. Sorbents (10 mg) were suspended in 10 mL of 350 mg/L $Cd^{2+}$ at pH of 5.0.

**2.4.2 Effect of initial cadmium concentration**

The adsorption isotherms were studied by varying the initial concentration of Cd from 0 to 373 ppm. Sorbents (10 mg) were suspended in 10 mL $Cd^{2+}$ at pH of 5.0 and the mixtures were shaken for 24 hours.

**2.4.3 Effect of initial pH of cadmium solution**

The 350 mg/L $Cd^{2+}$ was prepared in different pH (2, 2.5, 3, 4, 5, 6, 7) using 0.01M, 0.1 $HNO_3$ and NaOH. The adsorption process was carried out using 10 mg of sorbents in 10 mL of $Cd^{2+}$, and the mixtures were shaken for 24 hours.

# CHAPTER 3
# RESULTS AND DISCUSSION

## 3.1 Synthesis, characterization of the synthesized materials and their preliminary study on the removal of cadmium

Magnetic calcium phosphate composites were synthesized in the presence of citric acid via simple precipitation method. The synthesized materials were characterized by FTIR, XRD, elemental analysis, surface area analysis, TEM, SEM, DSC, and VSM. The optimized conditions of the synthesis process, including the order of adding starting materials, pH of the reaction mixture, and the initial Ca/P ratio were studied. Pristine Hap, Hap/citric, bare $Fe_3O_4$, and Hap/$Fe_3O_4$ were also synthesized and characterized for evaluating the performance of CPs/$Fe_3O_4$/citric composites. ACP could not be synthesized in the synthesis condition of this work because the phase was meta-stable and readily transformed to Hap.

### 3.1.1 Synthesis, characterization and cadmium adsorption capacities of Hap, Hap/citric, $Fe_3O_4$ and Hap/$Fe_3O_4$

The XRD patterns of Hap, Hap/citric, $Fe_3O_4$ and Hap/$Fe_3O_4$ were shown in Figure 3.1. Hap and Hap/citric contained pure Hap phase (JCPDS: PDF 74-0566). The difference was that the XRD pattern of Hap/citric had broader peaks, indicating lower crystallinity of Hap as the influence of citric acid. Hap/$Fe_3O_4$ had similar XRD pattern to that of Hap with the addition of three characteristic peaks of $Fe_3O_4$ at 35.60°, 57.21°, and 62.97° (JCPDS: PDF 86-1361). This result confirmed that the composite was comprised of Hap phase and $Fe_3O_4$ phase.

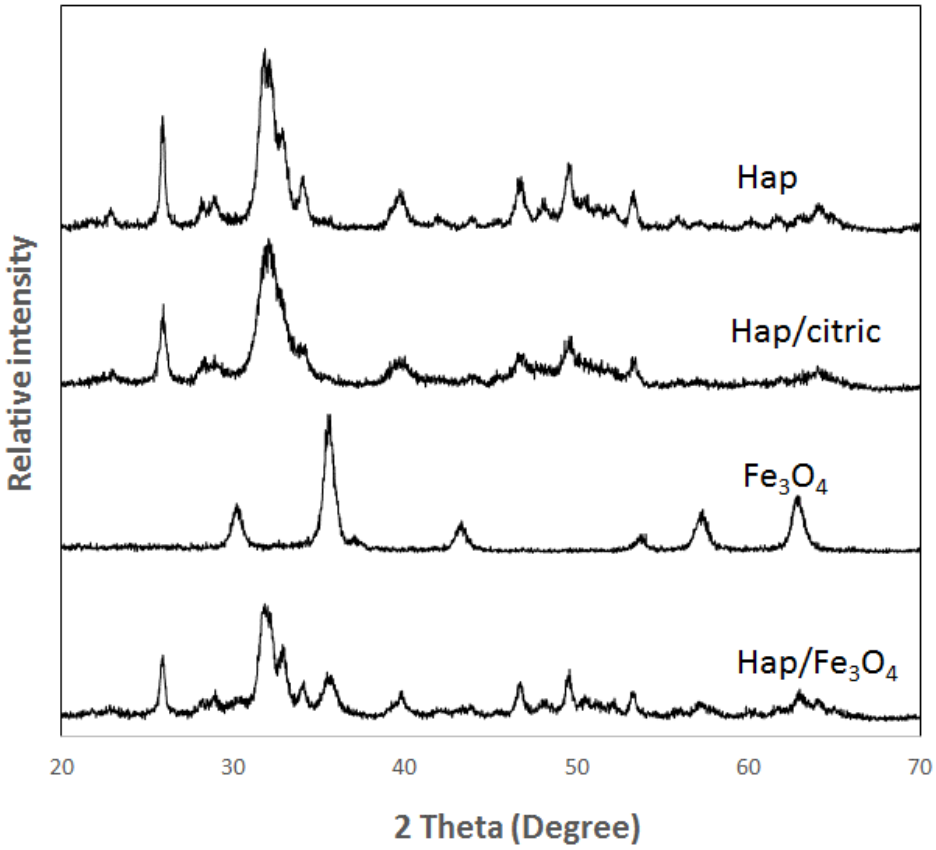


Figure 3.1 XRD patterns of Hap, Hap/citric, $Fe_3O_4$ and Hap/$Fe_3O_4$

These composites were also characterized by FITR (Figure 3.2). In the spectrum of Hap sample, the vibrational bands at *ca*. 1098, 1043, 957, 606 and 566 $cm^{-1}$ corresponded to $PO_4^{3-}$ vibration. The vibration bands at *ca*. 3424 and 636 $cm^{-1}$ are attributed to $OH^-$ groups. The bands at 1640 and 1381 $cm^{-1}$ corresponded to the adsorbed water and $CO_3^{2-}$ due to the dissolution of $CO_2$ during the synthesis process, respectively. These bands also appeared in the spectra of Hap/citric and Hap/$Fe_3O_4$. Only in the FTIR spectrum of Hap/citric, two broad additional bands around *ca*. 1595 and 1400 $cm^{-1}$ were found. They could be assigned as $n_{asym}(COO^-)$ and $n_{sym}(COO^-)$ of citrate ions, but these two bands overlapped with adsorbed water band and carbonate band, respectively.

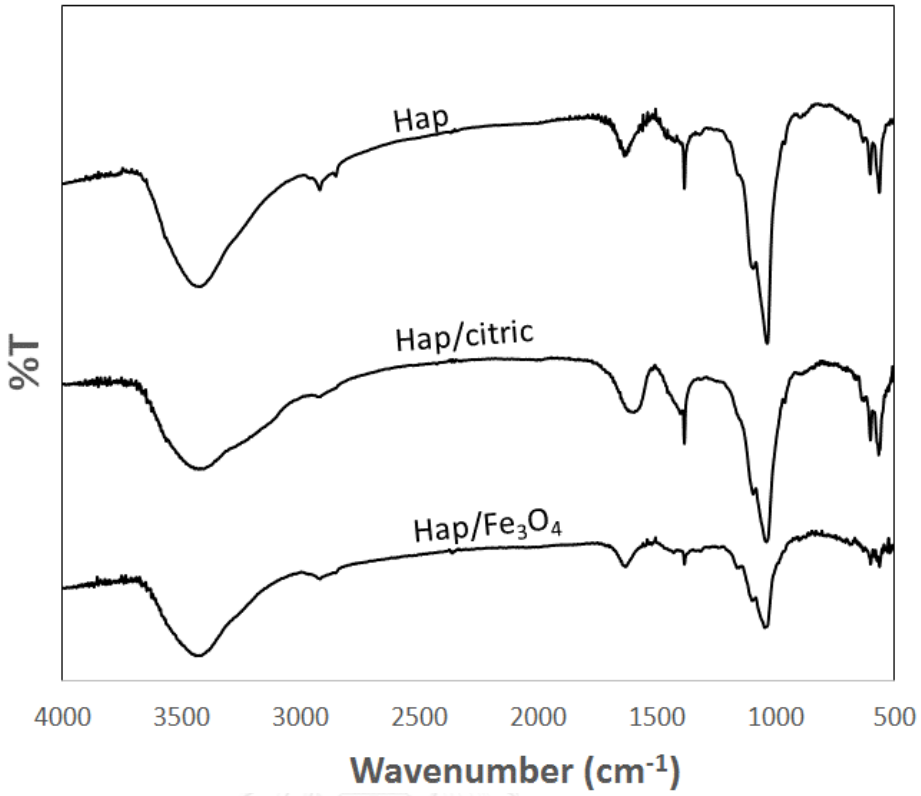


Figure 3.2 FTIR spectra of Hap, Hap/citric and Hap/$Fe_3O_4$

In addition to the FTIR results, the presence of citrate ions in the Hap/citric sample was confirmed by elemental analysis (Table 3.1). The carbon amount of 5.07% was detected in the Hap/citric sample, while those of Hap and Hap/$Fe_3O_4$ were 0.91% and 0.97%, respectively. The amount of citrate ions ($C_6H_5O_7^{3-}$) was calculated to be 13.3% in the Hap/citric sample. Adding citric acid in the synthesis and the existence of citrate ions in the Hap/citric final product enhanced the surface area of Hap by 1.9 times. To explain this, Hu *et al*. [45] proposed that citrate ions could bind strongly to calcium ions and create negative charges on the Hap surface. These negative charges repelled with phosphate ions and other Hap nuclei resulting in the inhibition of further crystal growth and the prevention of the particle aggregation. Besides citric acid, magnetite could also enhance the surface area of Hap by 1.4 times. This could be explained that $Fe_3O_4$ particles disturbed the crystals growth and prevented the aggregation of Hap nuclei. TEM images (Figure 3.3) clearly revealed the smaller particles of Hap/citric and Hap/$Fe_3O_4$ compared to those of Hap. The needle-like morphology of Hap-based materials was found in all samples. The size of those needles in

Hap/citric (12 - 30 nm) and Hap/$Fe_3O_4$ (13 – 29 nm) was smaller than that of pure Hap (31 -75 nm).

The nitrogen adsorption - desorption isotherm of Hap/citric possessed type IV according to the IUPAC classification, while those of Hap and Hap/$Fe_3O_4$ exhibited type II (Figure 3.4) [50]. This could indicate the micro-mesoporous structure of Hap/citric sample (pore size of 3.53 nm) and macroporous or non-porous structures of Hap and Hap/$Fe_3O_4$.

Cadmium adsorption capacities of Hap, Hap/citric, $Fe_3O_4$ and Hap/$Fe_3O_4$ were shown in table 3.1. The adsorption capacity (143 mg $g^{-1}$) of Hap/citric was quite high as compared to that of Hap (104.4 mg $g^{-1}$) that could attribute to its higher surface area. For Hap/$Fe_3O_4$, considering that it contained 71 wt% Hap and 17 wt% $Fe_3O_4$ (calculated from the calcium and iron in the digested sample), the calculated cadmium removal capacity was 73.8 (mg $g^{-1}$). The higher experimental value of 97.7 (mg $g^{-1}$) could be explained by the higher surface area of Hap/$Fe_3O_4$.

Table 3.1 Surface area, cadmium adsorption capacities and the weight percentages of calcium, phosphorus, and iron of Hap, Hap/citric and Hap/$Fe_3O_4$

| Samples | $S_{BET}$[a] ($m^2$ $g^{-1}$) | C[b] (wt%) | Ca[c] (wt%) | P[c] (wt%) | Fe[c] (wt%) | Ca/P[c] | Cadmium adsorption capacity[d] (mg $g^{-1}$) |
|---|---|---|---|---|---|---|---|
| Hap | 73.2 | 0.91 | 36.26 | 17.42 | 0 | 1.61 | 104.4 |
| Hap/citric | 138.7 | 5.07 | 34.26 | 15.34 | 0 | 1.74 | 143.3 |
| Hap/$Fe_3O_4$ | 103.5 | 0.97 | 28.26 | 13.19 | 12.44 | 1.63 | 97.7 |

[a] from $N_2$ isotherm using the BET model

[b] from elemental analysis

[c] Samples were digested and measured by ICP-OES

[d] The removal process was performed by suspending 10 mg of sorbent in 10 mL $Cd^{2+}$ 350 mg/L at pH of 5.0. The concentration of $Cd^{2+}$ was measured by ICP-OES

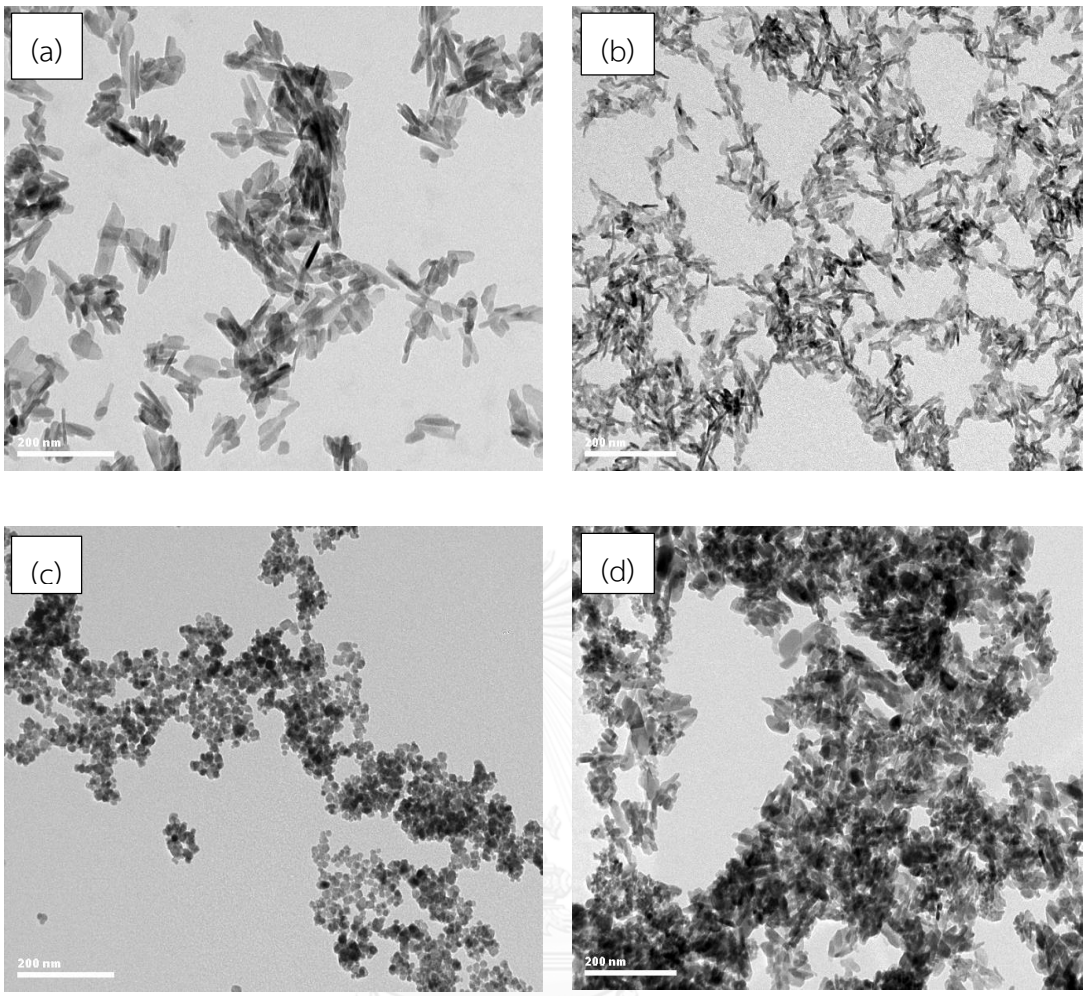


Figure 3.3 TEM images of Hap (a), Hap/citric (b), $Fe_3O_4$ (c) and Hap/$Fe_3O_4$ (d)

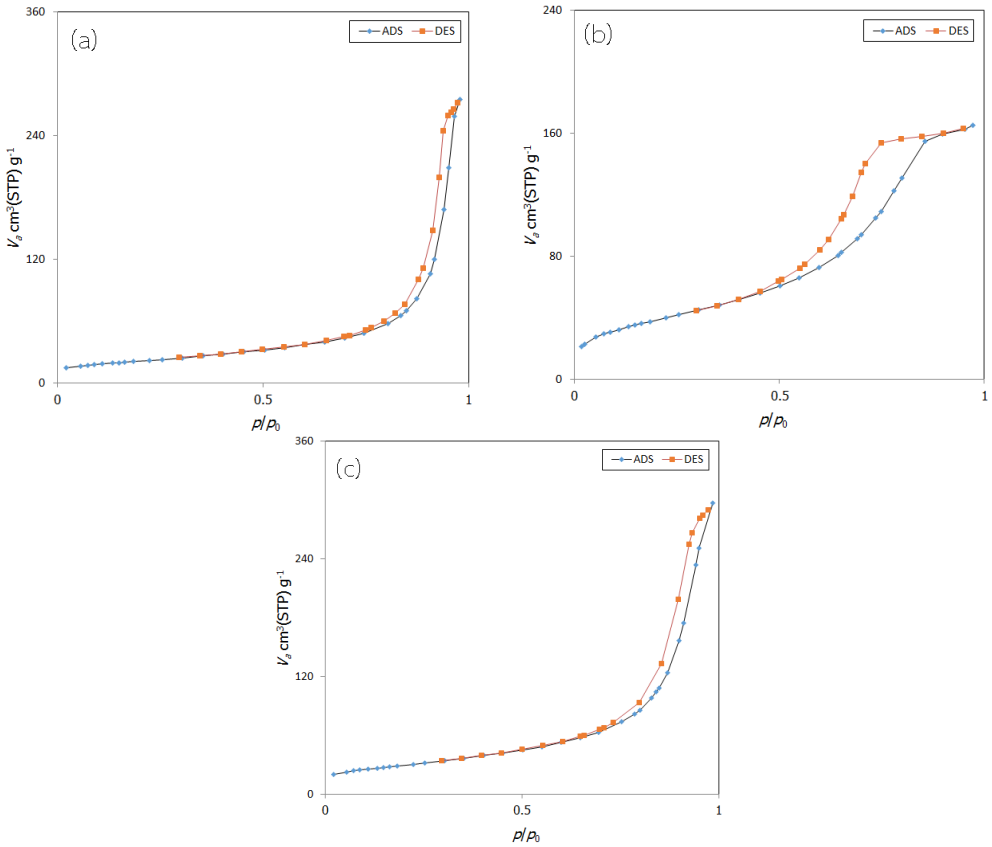


Figure 3.4. Nitrogen adsorption - desorption isotherms of Hap (a), Hap/citric (b) and Hap/$Fe_3O_4$ (c)

In addition, the experimental study about the effect of citric acid on magnetite was also set up. After adding citric acid to the formed $Fe_3O_4$, the nanoparticles were well dispersed in the aqueous solution and did not precipitate or accumulate under the influence of magnet. The stable suspension of magnetite nanoparticles would be useful in the synthesis of the composite materials next. Therefore, citric acid was then used as an additive in the synthesis of magnetic calcium phosphate materials.

**3.1.2 Synthesis, characterization and cadmium adsorption capacities of CPs/ $Fe_3O_4$/citric materials**

The optimized conditions of the synthesis process, including the order of adding starting materials, pH of the reaction mixture, and the initial Ca/P ratio were studied. The mole ratio of $Fe^{3+}/Ca^{2+}$ and citric acid/$Ca^{2+}$ of all CPs/$Fe_3O_4$/citric materials were 0.22 and 0.25, respectively.

### *3.1.2.1 Effect of order of adding the starting materials*

To determine the effect of citric acid to $Fe_3O_4$ and Hap, the order of adding the starting materials were varied and the final products were named in Table 3.2.

Table 3.2 Order of adding starting materials in the synthesis and the abbreviated names of the final products

| Order of adding starting materials | Abbreviated names |
|---|---|
| $Fe_3O_4 \longrightarrow Ca^{2+} \longrightarrow$ Solution of citric $\longrightarrow PO_4^{3-}$ | F – Ca – Ci – P |
| $Fe_3O_4 \longrightarrow$ Solution of citric acid + $PO_4^{3-} \longrightarrow Ca^{2+}$ | F – Ci+P – Ca |
| $Fe_3O_4 \longrightarrow$ Solution of citric acid $\longrightarrow Ca^{2+} + PO_4^{3-}$ | F – Ci – Ca+P |
| $Fe_3O_4 \longrightarrow$ Solution of citric acid $\longrightarrow Ca^{2+} - PO_4^{3-}$ | F – Ci – Ca – P |

The XRD patterns of these synthesized materials were shown in Figure 3.5. Similar to Hap/$Fe_3O_4$, these materials consisted of Hap phase and $Fe_3O_4$ phase. Furthermore, the FTIR spectra (Figure 3.6) of these Hap/$Fe_3O_4$/citric materials were similar to that of Hap/citric, indicating the presence of $PO_4^{3-}$, $OH^-$, and citrate ions.

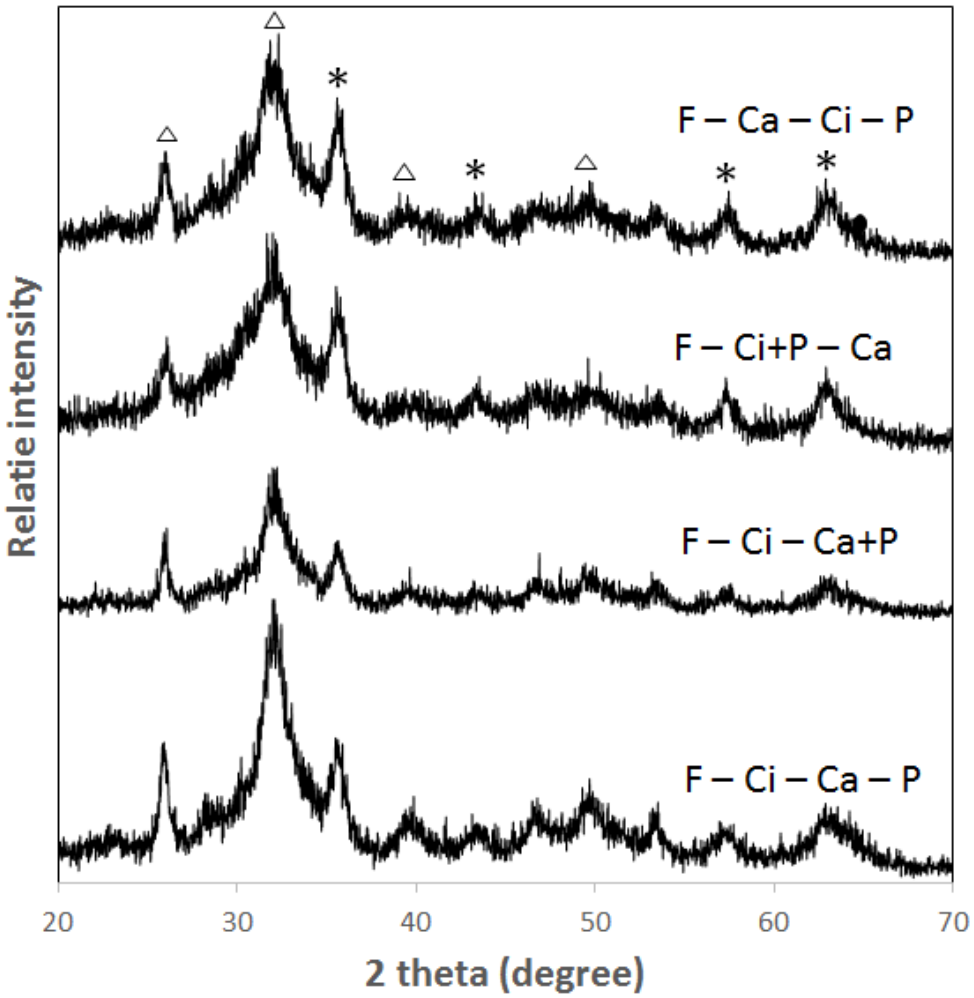


Figure 3.5 XRD patterns of Hap/$Fe_3O_4$/citric composites with different order of adding starting materials (△: Hap, *: $Fe_3O_4$)

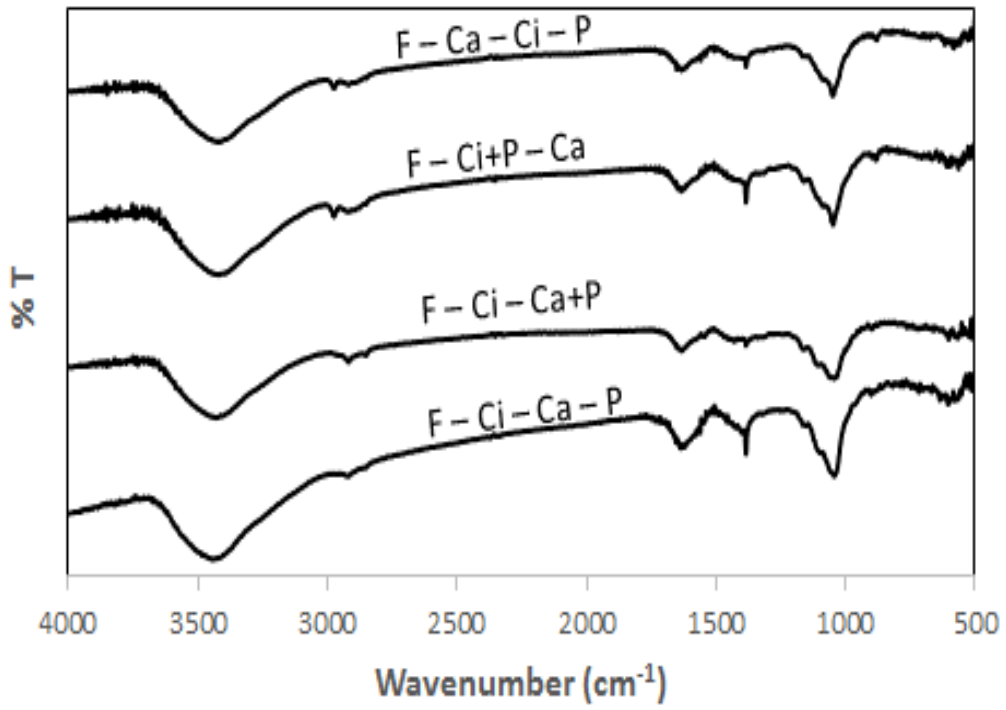


Figure 3.6 FTIR spectra of Hap/$Fe_3O_4$/citric composites with different order of adding starting materials

The specific surface area and the weight percentages of calcium, phosphorus, and iron in the materials were shown in table 3.3. According to the elemental analysis results, the percentages of citrate ions in the these composites were in the range of 11.9% - 14.9%. With the presence of citrate ions and magnetite, the surface area of all four materials were higher than both Hap/citric and Hap/$Fe_3O_4$. Moreover, the nitrogen adsorption – desorption isotherms of these four materials (Figure 3.7) belonged to type IV, indicating the micro-mesoporous structure (pore size in the range of 1.64 – 3.09). Notice that the highest specific surface area values were obtained when citric acid was added into $Fe_3O_4$ before Hap precipitated. These results indicated the ability of citric acid to stabilize magnetite nanoparticles and inhibit the growth of Hap as mentioned above.

The cadmium adsorption capacities of four Hap/$Fe_3O_4$/citric composites with different adding order of starting materials were summarized in Table 3.3. The capacities of these materials were relatively higher than both Hap/citric and Hap/$Fe_3O_4$.

Unlike that has been discussed in section 3.1.1, the capacities of these four materials did not relate to the surface area. The removal ability might also depend on other characteristics, such as crystallinities of the materials.

Table 3.3 Surface area, cadmium adsorption capacities and the weight percentages of calcium, phosphorus, and iron of Hap/$Fe_3O_4$/citric composites with different order of adding starting materials

| Samples | $S_{BET}$[a] ($m^2\ g^{-1}$) | C[b] (wt%) | Ca[c] (wt%) | P[c] (wt%) | Fe[c] (wt%) | Ca/P[c] | Cadmium adsorption capacity[d] (mg $g^{-1}$) |
|---|---|---|---|---|---|---|---|
| F – Ca – Ci – P | 167.3 | 5.67 | 21.25 | 10.57 | 11.40 | 1.59 | 181.4 |
| F – Ci+P – Ca | 177.5 | 5.51 | 22.23 | 10.84 | 10.60 | 1.59 | 195.9 |
| F – Ci – Ca+P | 208.3 | 4.52 | 24.82 | 11.70 | 11.40 | 1.64 | 149.0 |
| F – Ci – Ca – P | 182.5 | 4.76 | 22.95 | 11.56 | 10.87 | 1.53 | 131.5 |

[a] from $N_2$ isotherm using the BET model

[b] from elemental analysis

[c] Samples were digested and measured by ICP-OES

[d] The removal process was performed by suspending 10 mg of sorbents in 10 mL $Cd^{2+}$ 350 mg/L at pH of 5.0. The concentration of $Cd^{2+}$ was measured by ICP-OES

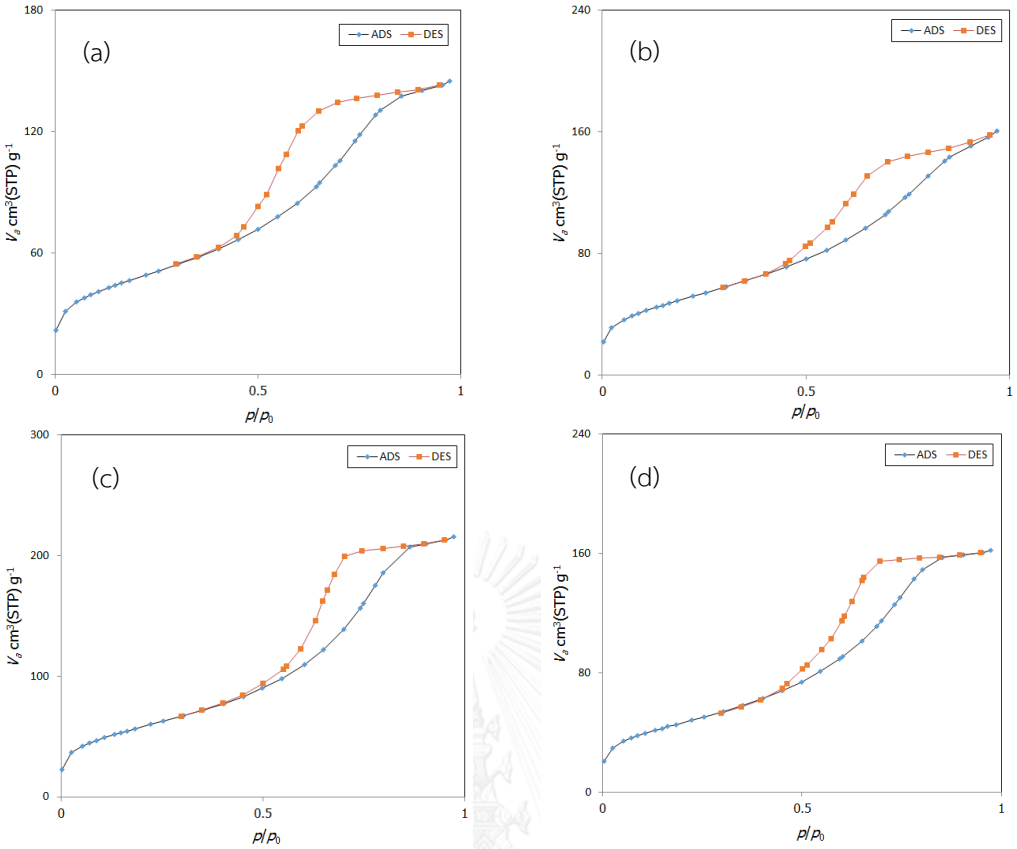


Figure 3.7. Nitrogen adsorption - desorption isotherms of Hap/$Fe_3O_4$/citric composites with different order of adding starting materials (F – Ca – Ci – P (a), F – Ci+P – Ca (b), F – Ci – Ca+P (c), and F – Ci – Ca – P (d))

In conclusion, by varying the order of adding starting materials, the phase of calcium phosphates was found to be Hap. These products had quite high surface area and relatively high cadmium adsorption capacities. The order [$Fe_3O_4$ – citric acid – $Ca^{2+}$ + $PO_4^{3-}$] was chosen to study the effect of pH due to the final product possessing the highest surface area.

### *3.1.2.2 Effect of pH of the reaction mixture*

The effect of pH of the reaction mixture after adding citric acid was studied due to the strong effect to the chelating ability of citric acid to calcium ions [44, 51]. These pH values were varied from lower than $pK_{a1}$ to higher than $pK_{a3}$ of citric acid, which was 2.3 - 9.5. The final products were named in Table 3.4.

Table 3.4 CPs/$Fe_3O_4$/citric composites synthesized at different pH and the abbreviated names of the final products

| Samples | Abbreviated names |
|---|---|
| $Fe_3O_4$ ⟶ Solution of citric acid ⟶ pH = 2.3 ⟶ $Ca^{2+}$ + $PO_4^{3-}$ | Citric – pH 2.3 |
| $Fe_3O_4$ ⟶ Solution of citric acid ⟶ pH = 4.0 ⟶ $Ca^{2+}$ + $PO_4^{3-}$ | Citric – pH 4.0 |
| $Fe_3O_4$ ⟶ Solution of citric acid ⟶ pH = 6.0 ⟶ $Ca^{2+}$ + $PO_4^{3-}$ | Citric – pH 6.0 |
| $Fe_3O_4$ ⟶ Solution of citric acid ⟶ pH = 6.7 ⟶ $Ca^{2+}$ + $PO_4^{3-}$ | Citric – pH 6.7 |
| $Fe_3O_4$ ⟶ Solution of citric acid ⟶ pH = 7.9 ⟶ $Ca^{2+}$ + $PO_4^{3-}$ | Citric – pH 7.9 |
| $Fe_3O_4$ ⟶ Solution of citric acid ⟶ pH = 9.5 ⟶ $Ca^{2+}$ + $PO_4^{3-}$ | Citric – pH 9.5 |

The XRD patterns of CPs/$Fe_3O_4$/citric composites synthesized at different pH were shown in Figure 3.8. All patterns shown the characteristic peaks of $Fe_3O_4$ (PDF 86-1361). At the pH higher than $pK_{a3}$ of citric acid (6.7-9.5), the XRD patterns also include the characteristic peaks of Hap (PDF 74-0566). While at the pH lower than $pK_{a3}$ (2.3-6.0), no other peak except those belongs to $Fe_3O_4$ appears. This could indicate the amorphous phase of calcium phosphates. The FTIR spectra of CPs/$Fe_3O_4$/citric (Figure 3.9) also indicated the presence of $PO_4^{3-}$, $OH^-$, and citrate ions mentioned in section 3.1.1 and 3.1.2.1.

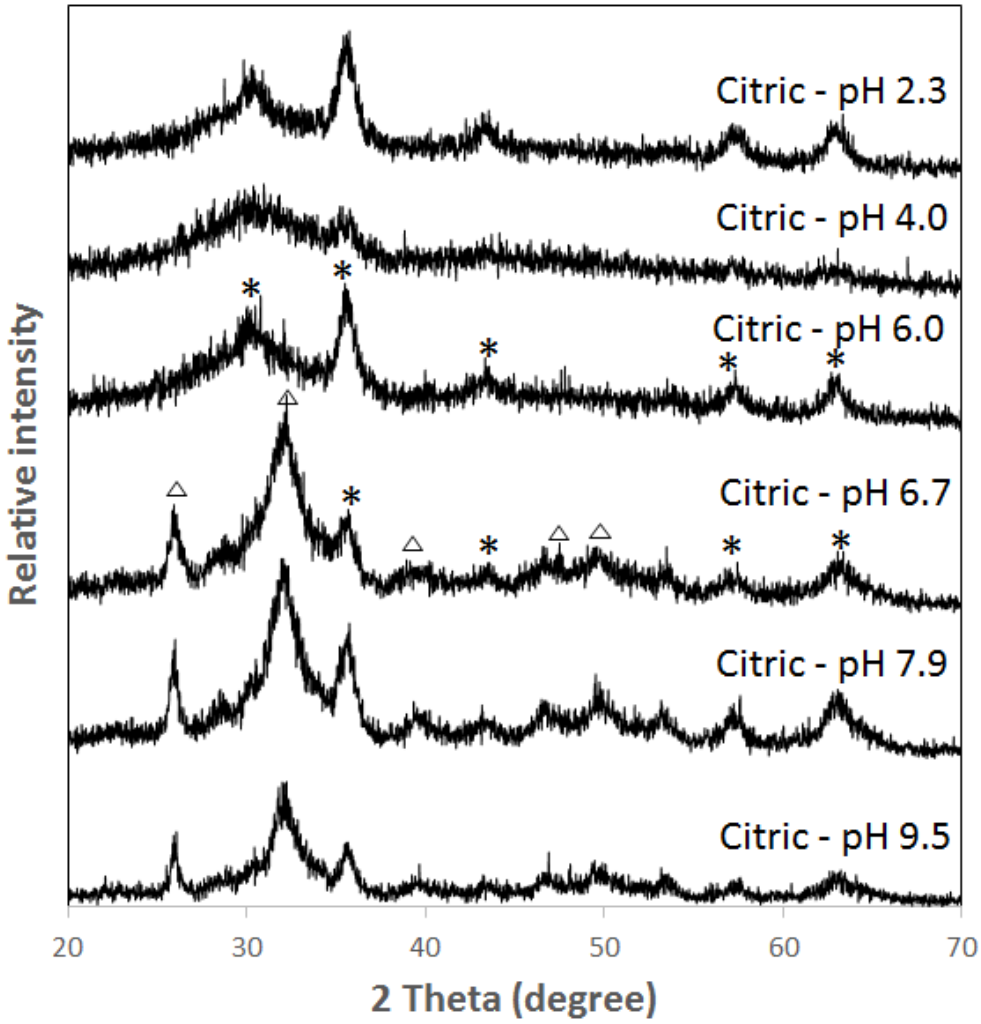


Figure 3.8 XRD patterns of CPs/$Fe_3O_4$/citric composites synthesized at different pH (△: Hap, *: $Fe_3O_4$)

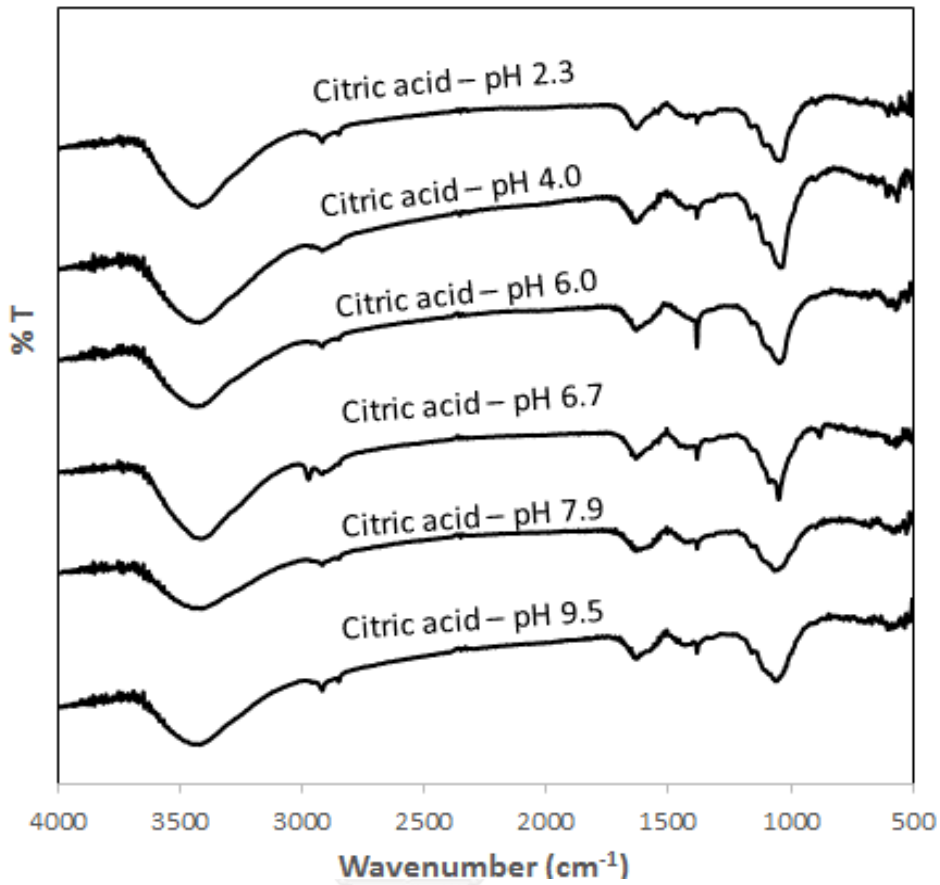


Figure 3.9 FTIR spectra of CPs/$Fe_3O_4$/citric composites synthesized at different pH

According to the percentages of carbon detected (Table 3.5), 11.8 wt% - 16.7 wt% citrate ions was found in these samples. It could be observed that ACP/$Fe_3O_4$/citric composites had lower specific surface area than those of Hap/$Fe_3O_4$/citric composites. However, the cadmium capacities of all ACP-based materials were much higher than those of Hap-based materials. The unrelated relationship between the surface area and cadmium removal ability could be explained by the different interaction of the water-containing ACP-based materials on the $N_2$ adsorption and on the $Cd^{2+}$ adsorption. For the determination of the specific surface area of ACP/$Fe_3O_4$/citric, the physical adsorption occurred bettween the solid and nitrogen gas molecules. Therefore, the bound water and inter-space water in the ACP/$Fe_3O_4$/citric materials would obstruct the adsorption of nitrogen molecules and thus reduced the specific surface area [27]. This hindrance was confirmed by the

nitrogen adsorption – desorption isotherms (Figure 3.10). These isotherms were classified as type II, exhibiting the non-porous materials. In the cadmium removal process, sorbents were suspended into the $Cd^{2+}$ solution. The metal ions are hydrophilic; therefore, the water in the structure of ACP-based materials could act as the medium for the adsorption process instead.

Furthermore, the large difference in the cadmium adsorption capacities between ACP composites and Hap composites pointed to the effect of crystallinity on the removal capacity. In the amorphous phase (ACP), $Ca^{2+}$ might be substituted by $Cd^{2+}$ from the solid sorbents easier than those in a crystalline phase (Hap) due to the presence of defects and dangling bonds normally found in an amorphous materials [52, 53]. The mechanism of cadmium removal will be discussed in the adsorption mechanism.

Table 3. 5 Surface area, cadmium adsorption capacities and the weight percentages of calcium, phosphorus, and iron of the CPs/$Fe_3O_4$/citric composites synthesized at different pH

| Samples | $S_{BET}$[a] ($m^2$ $g^{-1}$) | C[b] (wt%) | Ca[c] (wt%) | P[c] (wt%) | Fe[c] (wt%) | Ca/P[c] | Cadmium adsorption capacity[d] (mg $g^{-1}$) |
|---|---|---|---|---|---|---|---|
| Citric – pH 2.3 | 119.0 | 5.63 | 17.59 | 8.53 | 17.41 | 1.59 | 273.8 |
| Citric – pH 4.0 | 81.9 | 6.36 | 18.46 | 9.32 | 12.12 | 1.52 | 293.8 |
| Citric – pH 6.0 | 88.2 | 5.55 | 20.55 | 10.20 | 12.75 | 1.56 | 303.2 |
| Citric – pH 6.7 | 156.5 | 5.31 | 22.41 | 10.83 | 8.59 | 1.61 | 165.1 |
| Citric – pH 7.9 | 192.9 | 4.96 | 23.15 | 11.05 | 13.11 | 1.62 | 146.7 |
| Citric – pH 9.5 | 208.3 | 4.52 | 24.82 | 11.70 | 11.40 | 1.64 | 149.0 |

[a] from $N_2$ isotherm using the BET model

[b] from elemental analysis

[c] Samples were digested and measured by ICP-OES

[d] The removal process was performed by suspending 10 mg of sorbents in 10 mL $Cd^{2+}$ 350 mg/L at pH of 5.0. The concentration of $Cd^{2+}$ was measured by ICP-OES

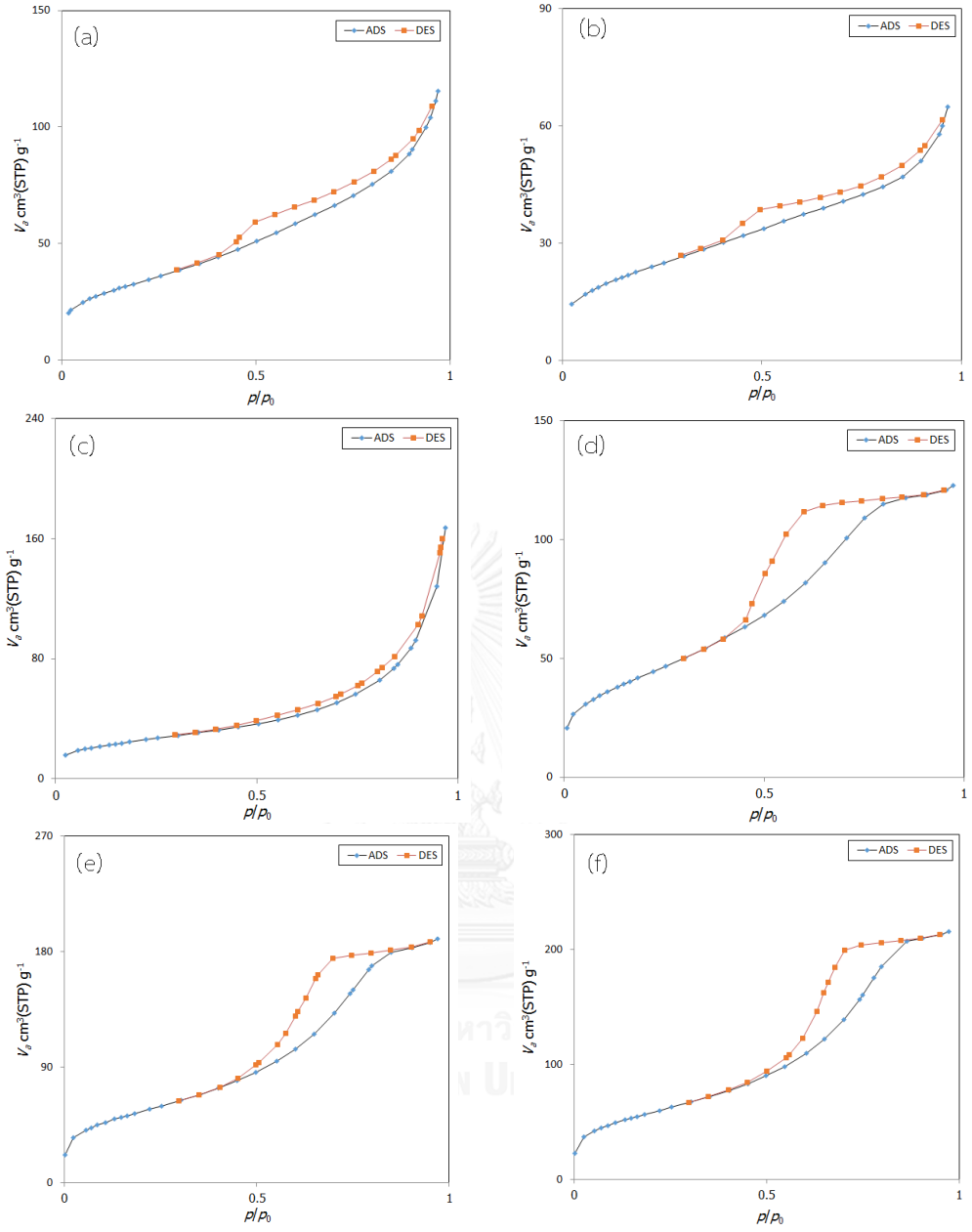


Figure 3.10. Nitrogen adsorption - desorption isotherms of CPs/$Fe_3O_4$/citric composites synthesized at pH 2.3 (a), 4.0 (b), 6.0 (c), 6.7 (d), 7.9 (e), and 9.5 (f)

TEM and SEM images of ACP/$Fe_3O_4$/citric (pH 6.0) and Hap/$Fe_3O_4$/citric (pH 9.5) (Figure 3.11) were chosen to represent the morphologies of the two types of magnetic calcium phosphates. The TEM image of ACP/$Fe_3O_4$/citric (Figure 3.11 (a)) suggested the particle aggregation. $Fe_3O_4$ particles were covered and linked by the irregular shape of ACP phase, resulting in the mossy surface as seen in the SEM image (Figure 3.11 (b)).

For Hap/$Fe_3O_4$/citric, the needle - shaped particles of hydroxyapatite and the nanosized $Fe_3O_4$ aggregated together (Figure 3.11 (c) and (d)).

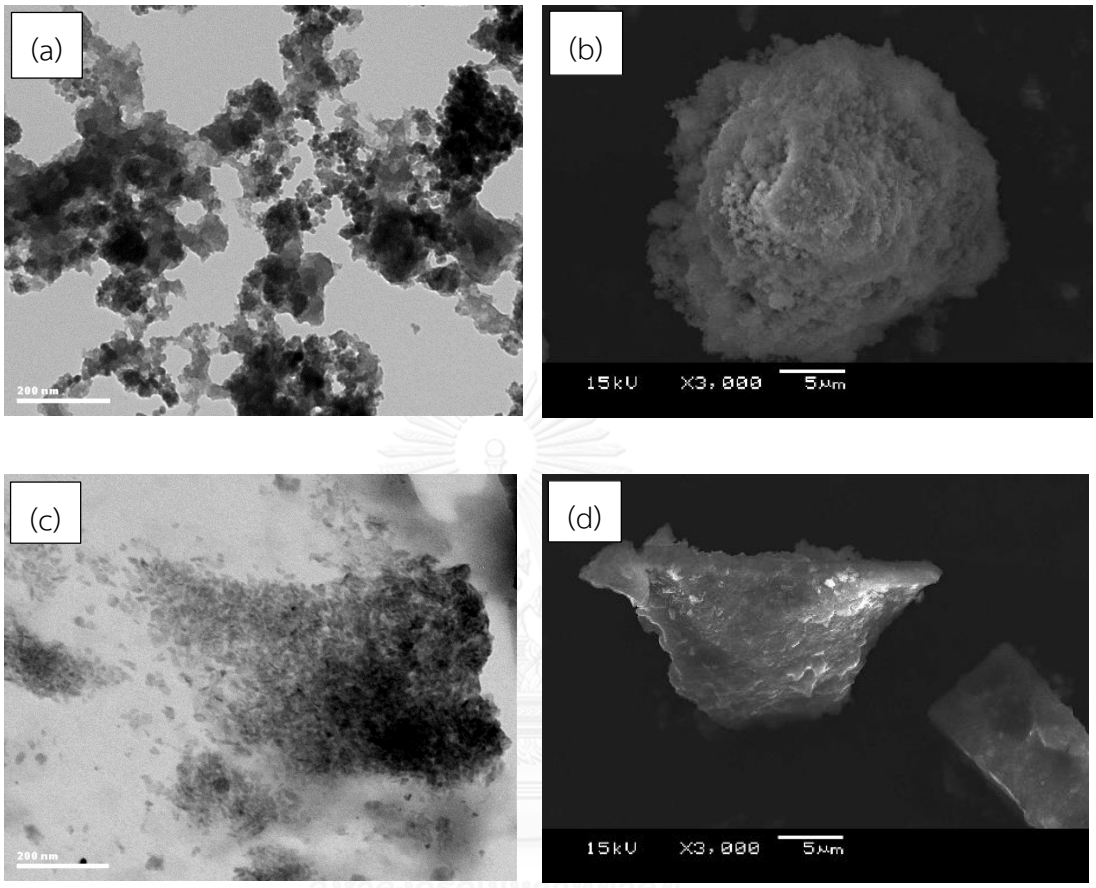


Figure 3.11 TEM image (a), SEM image (b) of ACP/$Fe_3O_4$/citric (pH 6.0), and TEM image (c), SEM image (d) Hap/$Fe_3O_4$/citric (pH 9.5)

As mentioned in chapter 1, amorphous calcium phosphates exists in the wide range of Ca/P ratio [27, 29]. Therefore, these ratios were studied in the range of 1.0 – 2.0. The order [$Fe_3O_4$ – solution of citric acid - pH 6.0 – $Ca^{2+}$ and $PO_4^{3-}$] was chosen to study the Ca/P ratio due to the achieved highest cadmium capacity in this section.

***3.1.2.3 Effect of Ca/P ratio***

The initial Ca/P ratio was varied and the final products were named in table 3.6.

Table 3.6 ACP/$Fe_3O_4$/citric composites with different Ca/P ratio and their abbreviated name of the final products

| Samples | Abbreviated names |
|---|---|
| $Fe_3O_4$ ⟶ Solution of citric acid ⟶ pH = 6.0 ⟶ $Ca^{2+}$ and $PO_4^{3-}$ with ratio Ca/P =1 | Ca/P =1.0 |
| $Fe_3O_4$ ⟶ Solution of citric acid ⟶ pH = 6.0 ⟶ $Ca^{2+}$ and $PO_4^{3-}$ with ratio Ca/P =1.5 | Ca/P =1.5 |
| $Fe_3O_4$ ⟶ Solution of citric acid ⟶ pH = 6.0 ⟶ $Ca^{2+}$ and $PO_4^{3-}$ with ratio Ca/P =1.67 | Ca/P =1.67 |
| $Fe_3O_4$ ⟶ Solution of citric acid ⟶ pH = 6.0 ⟶ $Ca^{2+}$ and $PO_4^{3-}$ with ratio Ca/P =2 | Ca/P =2.0 |

The FTIR spectra of these composites (Figure 3.12) indicated the presence of phosphate and citrate ions as discussed in previous sections. The XRD patterns of composites with different Ca/P ratio were shown in Figure 3.13. Only $Fe_3O_4$ phase appeared in all XRD patterns, indicating that the formation of calcium phosphate in different Ca/P ratio was ACP.

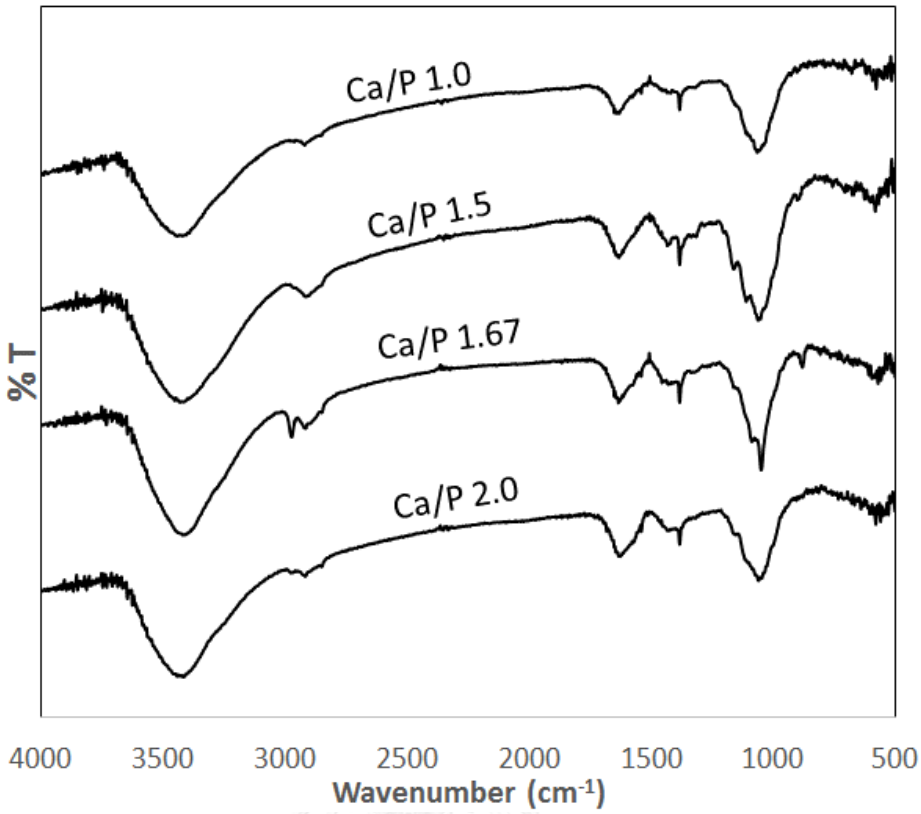


Figure 3.12 FTIR spectra of ACP/$Fe_3O_4$/citric composites with different Ca/P ratio

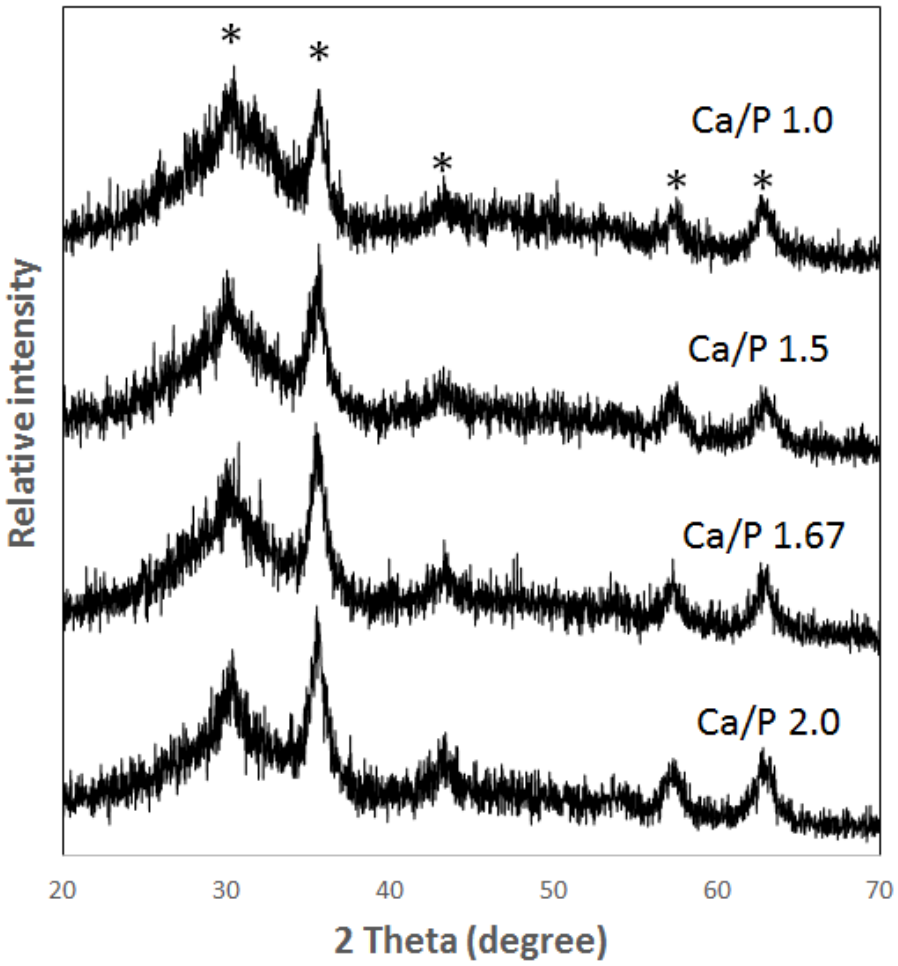


Figure 3.13 XRD patterns of ACP/$Fe_3O_4$/citric composites with different Ca/P ratio (*: $Fe_3O_4$)

The surface area values of all ACP-based composites (Table 3.7) were lower than those of all Hap-based composites in section 3.1.2.2. Moreover, the nitrogen adsorption – desorption isotherms belonged to type II indicating the non-porous materials (Figure 3.14). These results could also explained by the trapped water in the inter-space of clusters. It could be observed that ACP/$Fe_3O_4$/citric composites with different Ca/P ratio exhibited high cadmium removal ability. This result confirmed that the low crystalline calcium phosphates possessed high cadmium adsorption capacity. ACP/$Fe_3O_4$/citric (Ca/P ratio of 1.5) was chosen for further study because of having highest cadmium removal capacity.

Table 3.7 Surface area, cadmium adsorption capacities and the weight percentages of calcium, phosphorus, and iron of ACP/$Fe_3O_4$/citric composites with different Ca/P ratio

| Samples | $S_{BET}$[a] ($m^2$ $g^{-1}$) | C[b] (wt%)f | Ca[c] (wt%) | P[c] (wt%) | Fe[c] (wt%) | Ca/P[c] | Cadmium adsorption capacity[d] (mg $g^{-1}$) |
|---|---|---|---|---|---|---|---|
| Ca/P =1.0 | 117.6 | 4.12 | 21.86 | 13.24 | 10.79 | 1.27 | 256.9 |
| Ca/P =1.5 | 88.7 | 6.16 | 20.08 | 10.75 | 11.46 | 1.48 | 323.1 |
| Ca/P =1.67 | 88.2 | 6.52 | 22.41 | 10.83 | 8.59 | 1.61 | 303.2 |
| Ca/P =2.0 | 77.0 | 8.21 | 19.2 | 8.73 | 15.16 | 1.71 | 313.0 |

[a] from $N_2$ isotherm using the BET model

[b] from elemental analysis

[c] Samples were digested and measured by ICP-OES

[d] The removal process was performed by suspending 10 mg of sorbent in 10 mL $Cd^{2+}$ 350 mg/L at pH of 5.0. The concentration of $Cd^{2+}$ was measured by ICP-OES

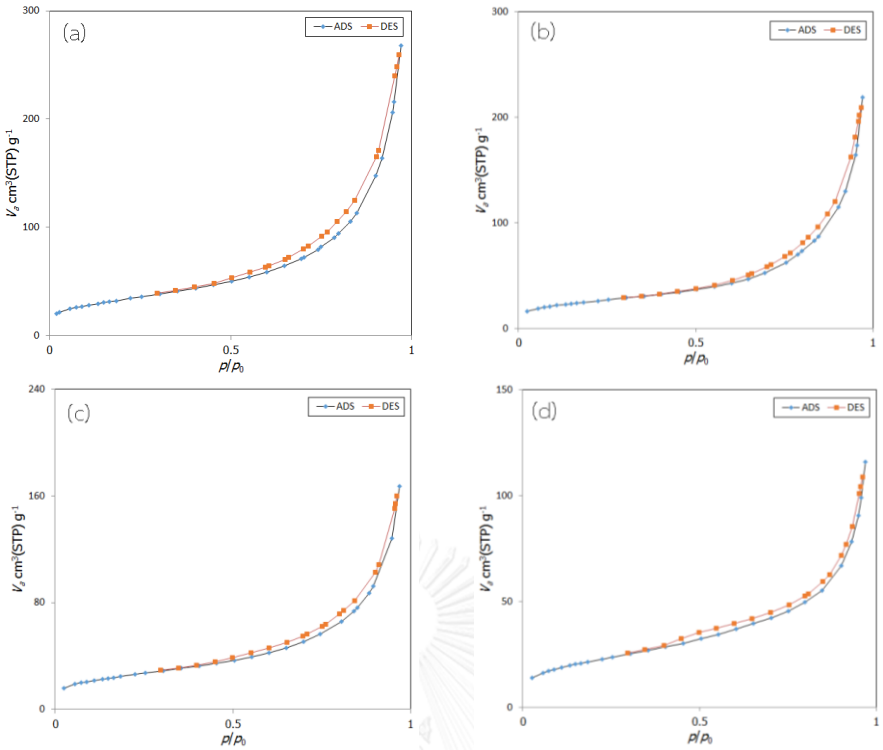


Figure 3.14. Nitrogen adsorption - desorption isotherms of ACP/$Fe_3O_4$/citric composites with Ca/P ratio of 1.0 (a), 1.5 (b), 1.67 (c), and 2.0 (d)

The TEM and SEM images of ACP/$Fe_3O_4$/citric (Ca/P 1.5) were represented in Figure 3.15. In the SEM images, similar to that of the ACP/$Fe_3O_4$/citric (Ca/P 1.67) sample in Figure 3.11, this magnetic amorphous calcium phosphate had the spherical shape that was surrounded by mossy particles. These mossy surface particles could be ACP deposited on the $Fe_3O_4$ surface. ACP particles could be observed clearly in the TEM images (Figure 3.15 (a) and 3.15 (b)). The irregular shape of ACP particles linked together and became random network and chain that covered the $Fe_3O_4$ particles. Therefore, the SEM images (Figure 3.15 (c) and 3.15 (d)) appeared as mossy particles that aggregated to larger particles.

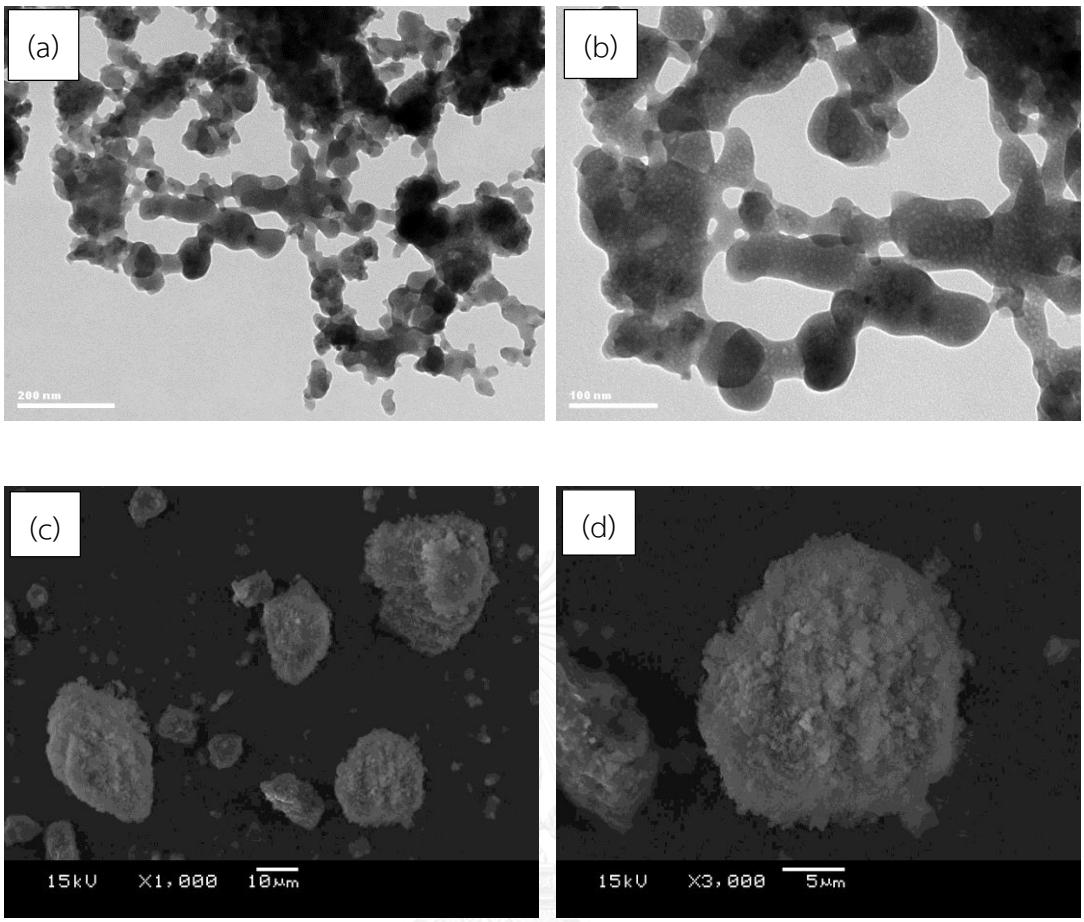


Figure 3.15 TEM (scale bar 200 nm) (a), (scale bar 100 nm) (b) and SEM (scale bar 10 µm) (c), (scale bar 5 µm) (d) of ACP/$Fe_3O_4$/citric composite (Ca/P 1.5)

In conclusion, among three parameters varied in the synthesis process, the pH of the reaction mixture was the only factor affecting the formation of different phases of calcium phosphates. ACP was yielded at the pH lower than $pK_{a3}$ of citric acid (2.3 - 6.0), and Hap was promoted at the pH higher than $pK_{a3}$ of citric acid (6.7 - 9.5). Higher cadmium capacity was achieved from the materials having lower crystallinities.

The magnetic properties of $Fe_3O_4$, Hap/$Fe_3O_4$, Hap/$Fe_3O_4$/citric and ACP/$Fe_3O_4$/citric were investigated (Figure 3.16). The four curves exhibited nearly zero values of magnetic remanence and coercivity, showing its superparamagnetic property [54]. The superparamagnetic behavior was expected for the magnetite particles having 15 nm in diameter [33] (TEM image Figure 3.3 (c)). The saturation magnetization ($M_s$) parameter of $Fe_3O_4$ was 61.4 (emu $g^{-1}$), while those of Hap/ $Fe_3O_4$, Hap/$Fe_3O_4$/citric and ACP/$Fe_3O_4$/citric were 10.64 (emu $g^{-1}$), 8.94 (emu $g^{-1}$), and 7.79 (emu $g^{-1}$), respectively. The reason of the lower saturation magnetization values of the composites than bare

magnetite was due to the non-magnetic phase of ACP or Hap separated the magnetite particles from each other. Therefore, under an external magnetic field, the magnetic induction among different magnetic domains was interrupted by non-magnetic phase [35, 48, 55]. Nonetheless, according to their saturation magnetization, these composites possessed a potential for convenient separation using an external magnetic field.

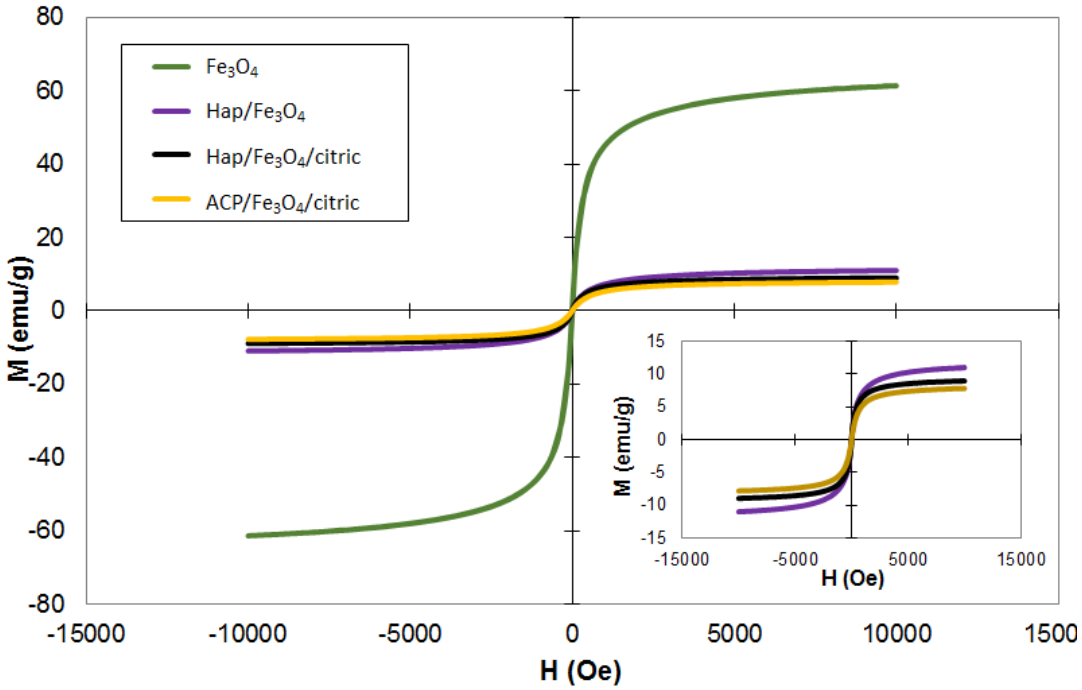


Figure 3.16. Magnetization hysteresis curves of $Fe_3O_4$, Hap/$Fe_3O_4$, Hap/$Fe_3O_4$/citric (pH 9.5) and ACP/$Fe_3O_4$/citric (Ca/P 1.5) (The inset shows the low field region of the magnetization curves of Hap/$Fe_3O_4$, Hap/$Fe_3O_4$/citric and ACP/$Fe_3O_4$/citric)

### 3.2 Mechanism proposed for the synthesis process

The schematic illustration of the formation of ACP/$Fe_3O_4$/citric and Hap/$Fe_3O_4$/citric was shown in Figure 3.17. There were two types of the formation of magnetic calcium phosphates depending on of the range of pH after adding citric during the synthesis process.

In the pH range lower than $pK_{a3}$ of citric acid (lower than 6.39), $Fe_3O_4$ had positive surface charge [56]. Thus, the electrostatic interaction between negative charge of the partial deprotonated species ($H_2C_6H_5O_7^-$ and $HC_6H_5O_7^{2-}$) of citric acid and positive charge on $Fe_3O_4$ surface was formed. Therefore, the anions were coated on

the surface of $Fe_3O_4$ and acted as steric stabilization of magnetite. After that, when $Ca^{2+}$ and $PO_4^{3-}$ were added, another end of the anions bound with $Ca^{2+}$, linking $Ca^{2+}$ to the surface of magnetite particles. As a result, the $Ca^{2+}$ ions were dispersed on the surface of magnetite, and the meta-stable phase of amorphous calcium phosphate was formed and maintained. Synthesis of calcium phosphates without magnetite or citric acid in similar conditions always yields the Hap phase (Hap/$Fe_3O_4$ and Hap/citric mentioned in section 3.1.1). The co-operation of magnetite and citrate species; therefore, was needed for the stability of ACP.

On the order hand, in the range of pH higher than $pK_{a3}$ of citric acid (6.7-9.5), the charge on the surface of magnetite particles became negative or less positive. Therefore, the interaction between fully-deprotonated citrate ions ($C_6H_5O_7^{3-}$) and magnetite surface became weaker. Citrate ions bound and chelated strongly with $Ca^{2+}$ ions, and the crystalline phase of Hap particles were formed and deposited or aggregated with magnetite particles. The founding of stronger chelation between citrate and $Ca^{2+}$ at higher pH was supported with the reported binding constant of citrate ions and $Ca^{2+}$ ($K=7.4x10^3$) at the pH higher than 6.39 and K=832 or K=28.2 at the pH lower than 6.39 [44].

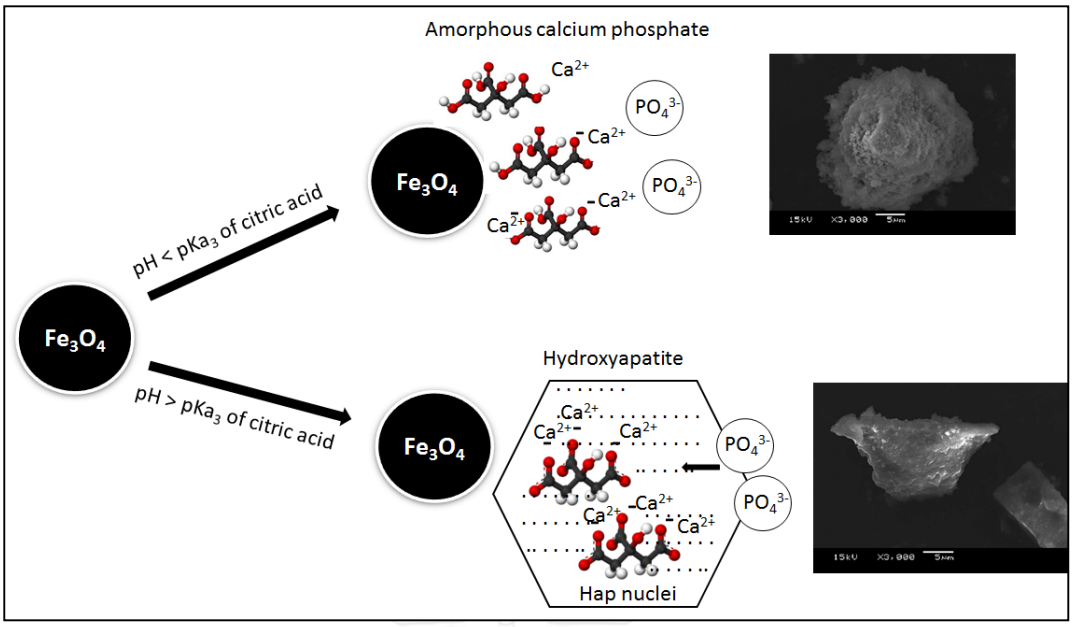


Figure 3.17 Schematic illustration of the formation of ACP/$Fe_3O_4$/citric and Hap/$Fe_3O_4$/citric

In order to understand more how citrate ions bonded in the materials, DSC technique was performed from 30°C to 450°C. The DSC curves of Hap, Hap/$Fe_3O_4$, Hap/citric, Hap/$Fe_3O_4$/citric (pH 9.5), and ACP/$Fe_3O_4$/citric (Ca/P 1.67 and 1.5) were presented in Figure 3.18. Hap and Hap/$Fe_3O_4$ samples were stable until 450 °C as no peak was observed. For the other samples containing citrate ions, the endothermic peaks in range of 143°C – 167°C corresponding to the melting temperature of citrate ions appear [57]. The shift of melting point could predict the bonding strength of citrate ions within its surroundings: Hap/citric > Hap/$Fe_3O_4$/citric > ACP/$Fe_3O_4$/citric. This could be explained that citrate ions could bind with crystalline phase of Hap in more orderly fashion, as compared to the composites. With the same reason, the random arragement of amorphous phase would shift the melting point to the lowest temperature.

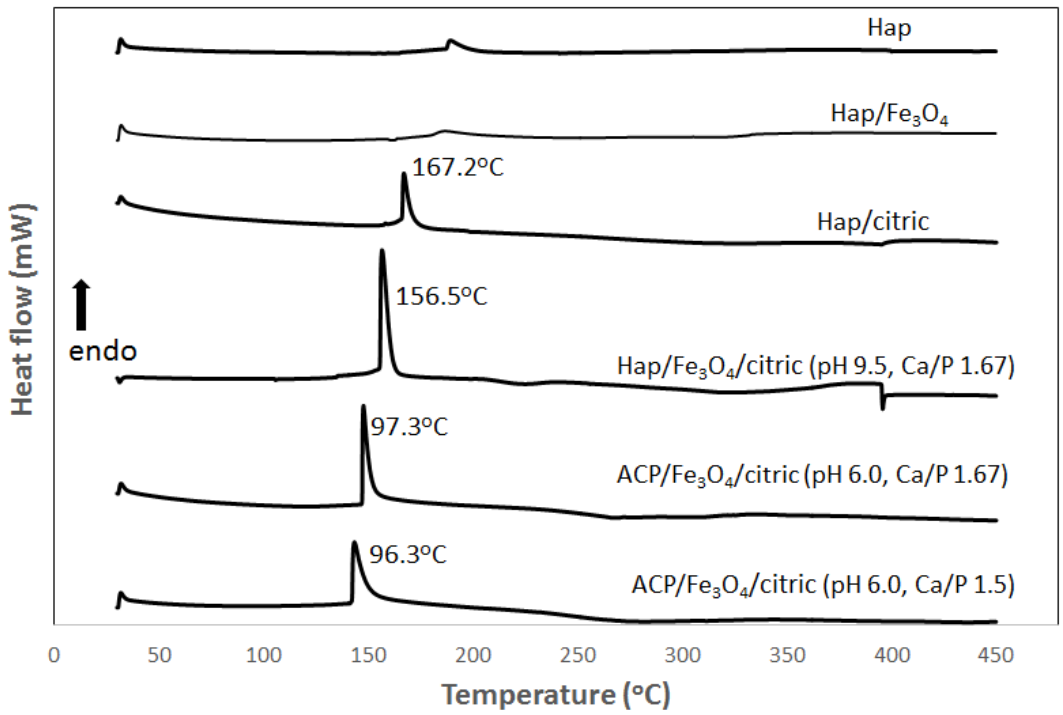


Figure 3.18 DSC curves of Hap, Hap/$Fe_3O_4$, Hap/citric, and the CPs/$Fe_3O_4$/citric composites

### 3.3 Adsorption study

The properties of ACP/$Fe_3O_4$/citric (Ca/P 1.5) in $Cd^{2+}$ adsorption, including the adsorption kinetics and adsorption behavior at equilibrium were studied. The adsorption mechanism was also investigated.

#### 3.3.1 Adsorption kinetics

The adsorption of $Cd^{2+}$ by the synthesized materials was observed at different contact time varied from 5 to 420 minutes (Figure 3.19). The adsorption occurred rapidly in the first 40 minutes and reached the equilibrium after 2 hours.

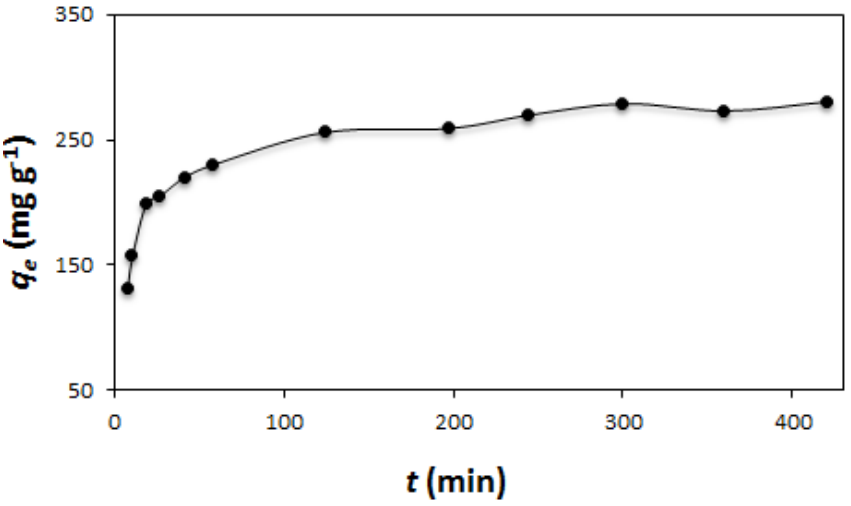


Figure 3.19 Effect of contact time on the uptake of $Cd^{2+}$ by ACP/$Fe_3O_4$/citric (Ca/P 1.5)

In order to determine the rate of the adsorption process, the pseudo-first order model (Eq.1) and pseudo-second order model (Eq.2) [35] were applied to the experimental kinetics data. The adsorption capacities (mg g$^{-1}$) observed at contact time *t*, and at equilibrium were presented by the variables $q_t$ and $q_e$, respectively. The pseudo-first order rate constant ($k_1$) and pseudo-second order rate constant ($k_2$) were determined by linear plot of the experimental data. The linear fit of experimental data obtained using pseudo-first-order and pseudo-second-order were shown in Figure 3.20 and Figure 3.21, respectively. The adsorption kinetics parameters were calculated and represented in Table 3.8. It was observed that the kinetics data were fitted with the pseudo-second-order model better than the pseudo-first-order model. The adsorption capacity at equilibrium calculated using pseudo-second order model ($q_{e,cal}$) was 285.7 mg g$^{-1}$, which was close to the experimental value ($q_{e,exp}$) of 272.3 mg g$^{-1}$, indicating a good fit of the model to the experimental data.

$$\log(q_e - q_t) = \log q_e - \frac{k_1}{2.303} t \qquad (1)$$

$$\frac{t}{q_t} = \frac{1}{k_2 q_e^2} + \frac{t}{q_e} \qquad (2)$$

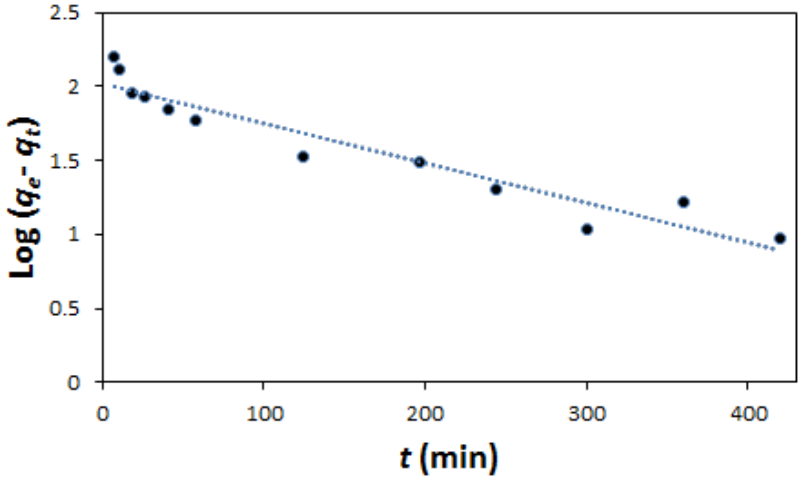


Figure 3.20 Linear plot of experimental data obtained using pseudo-first-order model

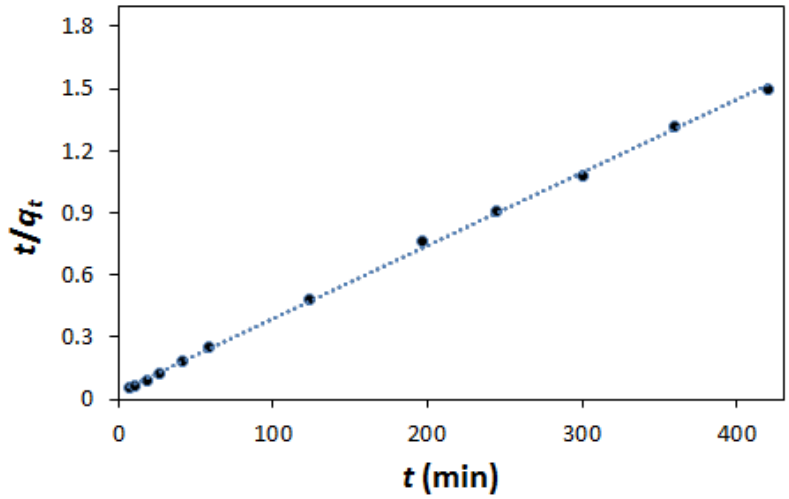


Figure 3.21 Linear fit of experimental data obtained using pseudo-second-order model

Table 3.8 Kinetics parameters of the adsorption of $Cd^{2+}$ on ACP/$Fe_3O_4$/citric (Ca/P 1.5)

| $q_{e,exp}$ (mg $g^{-1}$) | Pseudo-first-order | | | Pseudo-second-order | | |
|---|---|---|---|---|---|---|
| | $k_1$ (g $mg^{-1}$ $min^{-1}$) | $q_{e,cal}$ (mg $g^{-1}$) | $R^2$ | $k_2$ (g $mg^{-1}$ $min^{-1}$) | $q_{e,cal}$ (mg $g^{-1}$) | $R^2$ |
| 272.3 | $3.2x10^{-4}$ | 285.7 | 0.999 | $6.2x10^{-3}$ | 103.6 | 0.914 |

### 3.3.2 Adsorption isotherms

To investigate the adsorption behavior at equilibrium, the adsorption isotherms experiments were performed. The plot of cadmium adsorbed on ACP/$Fe_3O_4$/citric (Ca/P 1.5) was shown in Figure 3.22. The cadmium adsorption capacity increased with the increasing cadmium initial concentration.

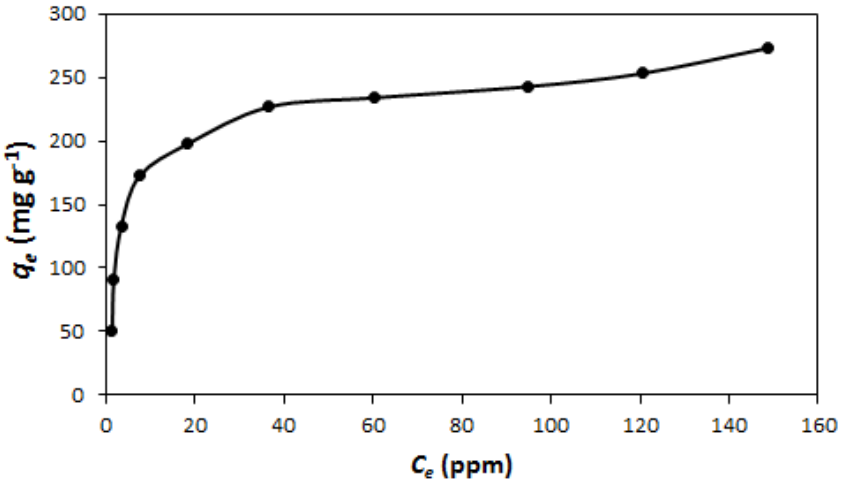


Figure 3.22 Adsorption isotherms of $Cd^{2+}$ by ACP/$Fe_3O_4$/citric (Ca/P 1.5)

The Langmuir (Eq.3) and Freundlich (Eq.4) isotherm equations [14, 32] were applied to analyze the adsorption behavior of this material. The Langmuir constant related to energy of adsorption ($K_L$), adsorbent maximum adsorption capacity ($q_m$), Freundlich constant ($n$) and a constant related to adsorption capacity ($K_f$) could be calculated from the linear equation obtained from experimental data.

$$\frac{C_e}{q} = \frac{C_e}{q_m} + \frac{1}{bq_m} \qquad (3)$$

$$\log q = \log K_f + \frac{1}{n}\log C_e \qquad (4)$$

The linear plot of Langmuir isotherm and Freundlich isotherm models were shown in Figure 3.23 and Figure 3.24, respectively. The Langmuir and Freundlich correlation coefficients and constants were calculated and shown in Table 3.9. According to the results, the Langmuir model fitted with the obtained adsorption data

better than Freundlich model. The Langmuir constant was 0.17 L $mg^{-1}$ and the maximum adsorption capacity was 270.3 mg $g^{-1}$. These results revealed that the adsorption of $Cd^{2+}$ ions on ACP/$Fe_3O_4$/citric occurred through chemisorption or likely cation exchange mechanism. The reaction of the sorbent and sorbate only took place on the active sites ($Ca^{2+}$) on the surface of materials and therefore, the monolayer adsorption was observed.

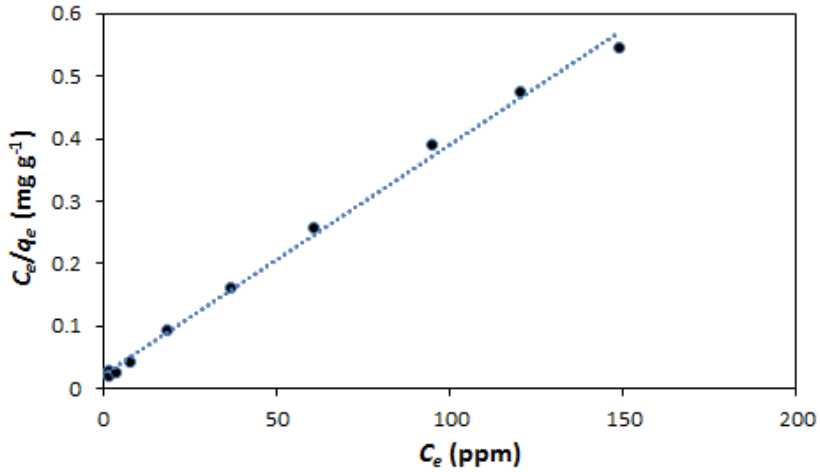


Figure 3.23 Linear fit of experiment data obtained using Langmuir model

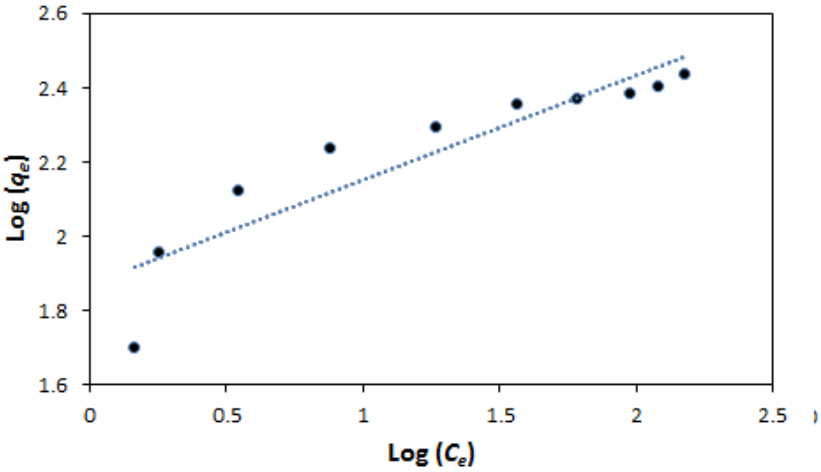


Figure 3.24 Linear fit of experiment data obtained using Freundlich model

Table 3.9 Langmuir and Freundlich correlation coefficients and constants of cadmium adsorption by ACP/$Fe_3O_4$/citric (Ca/P 1.5)

| Langmuir isotherm model | | | Freundlich isotherm model | | |
|---|---|---|---|---|---|
| $q_m$ (mg $g^{-1}$) | $K_L$ (L $mg^{-1}$) | $R^2$ | $K_f$ | $n$ | $R^2$ |
| 270.3 | 0.17 | 0.996 | 72.8 | 3.42 | 0.818 |

The capacity of the ACP/$Fe_3O_4$/citric in $Cd^{2+}$ ions adsorption was compared with those of other materials (Table 3.10). The ACP/$Fe_3O_4$/citric composite obtained by the proposed method showed relatively high adsorption capacity. When compared to crystalline hydroxyapatite, the amorphous calcium phosphate provided higher adsorption capacity. In an amorphous materials, there were defects and dangling bonds [52, 53, 58, 59] and $Ca^{2+}$ ions might be released and replaced by $Cd^{2+}$ ions easier than those in a crystalline phase. Therefore, the materials having lower crystallinities exhibited higher $Cd^{2+}$ adsorption capacity. This evidence makes amorphous calcium phosphate an interesting materials in respect to its ion exchange capacity. Even though, the ACP/$Fe_3O_4$/citric shown less adsorption capacity than pure amorphous calcium phosphate due to the presence of the magnetic particles, it had the advantage of convenient adsorbent separation.

Table 3.10 The comparison of cadmium adsorption capacities of this work with other works

| Materials | Method for the preparation | Cadmium adsorption capacity (mg $g^{-1}$) | References |
|---|---|---|---|
| Hydroxyapatite | Precipitation | 67.56* | [17] |
| Hydroxyapatite | Commercial synthesis | 66.54 | [15] |
| Hydroxyapatite | Hydrothermal technique | 260.42 | [14] |
| Hydroxyapatite/$Fe_3O_4$ | Precipitation | 220.8* | [13] |
| Amorphous calcium phosphate | Microwave-assisted hydrothermal method | 366 | [4] |
| ACP/$Fe_3O_4$/citric (Ca/P 1.5) | One-pot synthesis | 270 | This work |

*calculated from the published paper

### 3.3.3 Mechanism of adsorption process

In order to confirm the adsorption mechanism, the release of $Ca^{2+}$ from materials into the solutions during the adsorption of $Cd^{2+}$ was monitored. The relationship between the amount of $Ca^{2+}$ released and the amount of $Cd^{2+}$ adsorbed was investigated and shown in Figure 3.25. The results indicated that the amount of $Cd^{2+}$ adsorbed on the materials was directly proportional to that of $Ca^{2+}$ released from the materials. Moreover, the ratio of $C_{Cd}/C_{Ca}$ in a range from 0.77 to 1.15 was close to unity.

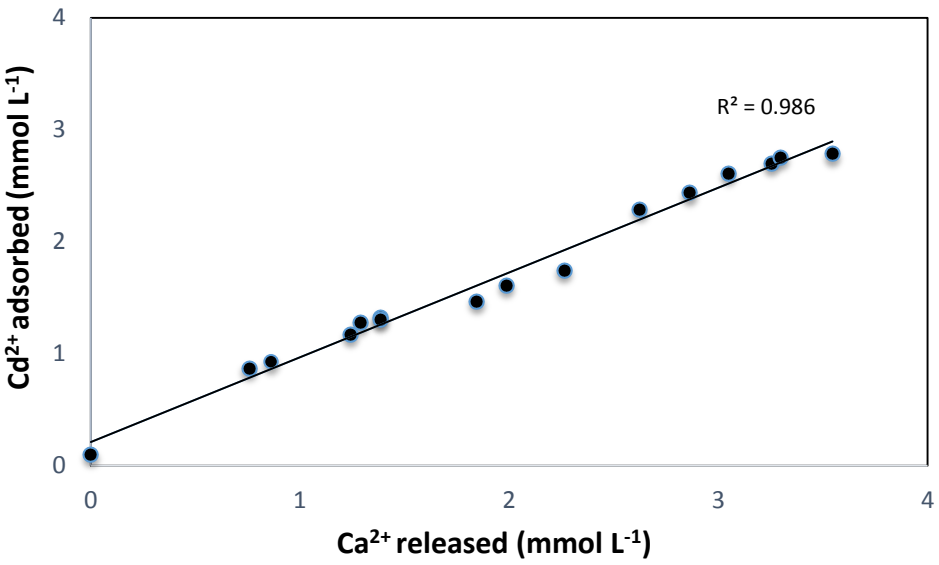


Figure 3.25 The relationship between the concentration of $Cd^{2+}$ adsorbed and the concentration of $Ca^{2+}$ released from adsorbents into the solution

Furthermore, the structures of materials before and after the adsorption process were observed by XRD. The XRD patterns before and after removing cadmium of ACP/$Fe_3O_4$/citric (Ca/P 1.5) and Hap/$Fe_3O_4$/citric (pH 6.7) were chosen as representatives (Figure 3.26). The XRD patterns of the adsorbents after being used in cadmium adsorption were similar to those of the original materials. This result indicated that the structures of magnetic calcium phosphate materials were maintained after the adsorption process. With the unchanged structure and the direct ration of $Cd^{2+}$ and $Ca^{2+}$ in agreement with other researches [4, 14, 17], this work confirmed the exchange mechanism between $Ca^{2+}$ in the magnetic calcium phosphates and $Cd^{2+}$ in the solution as shown in equation (5).

$$[CPs\text{-}Ca^{2+} + Cd^{2+} \longrightarrow CPs\text{-}Cd^{2+} + Ca^{2+}] \qquad (5)$$

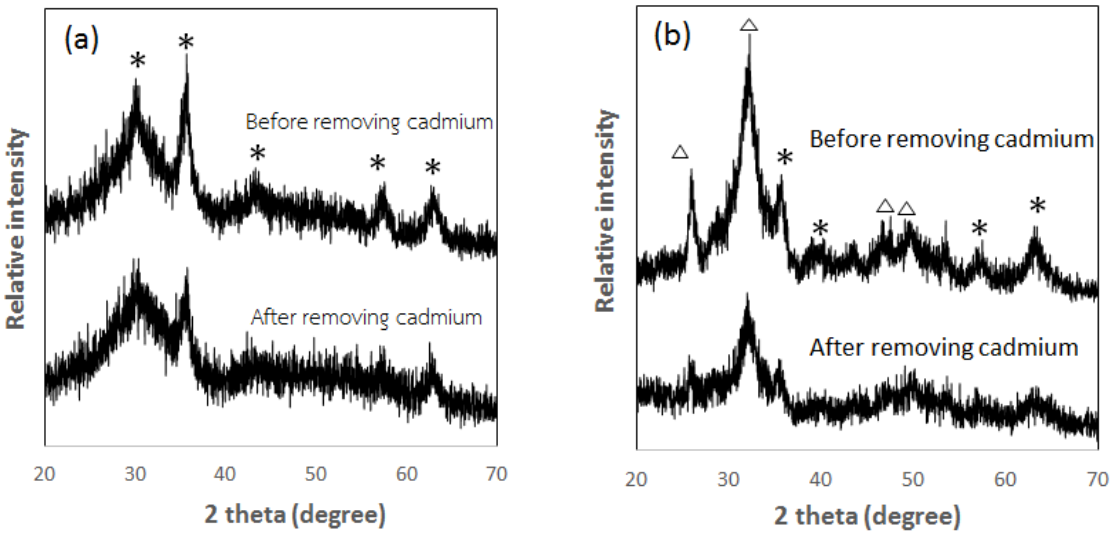


Figure 3.26 XRD patterns before and after removing cadmium of ACP/$Fe_3O_4$/citric (a), and Hap/$Fe_3O_4$/citric (b) (△: Hap, *: $Fe_3O_4$)

### 3.3.4 Effect of initial pH of cadmium solution

The effect of initial pH of $Cd^{2+}$ solution on cadmium removal ability of ACP/$Fe_3O_4$/citric (Ca/P) was studied in the range of 2 to 7 (Figure 3.27). From pH 3 to 7, the cadmium adsorption capacity remained constant. This indicated that pH has no effect on the $Ca^{2+}/Cd^{2+}$ exchange mechanism. With the same amount of $Ca^{2+}$ in the materials could release into the solution and the same amount of $Cd^{2+}$ in the solution were available to be adsorbed, the ACP/$Fe_3O_4$/citric (Ca/P 1.5) exhibited the remained constant of cadmium removal ability in this range of pH. The dramatic drop of cadmium adsorption capacity when the initial pH of the $Cd^{2+}$ solution became lower than 3 was due to the dissolution of ACP in strong acidic solution.

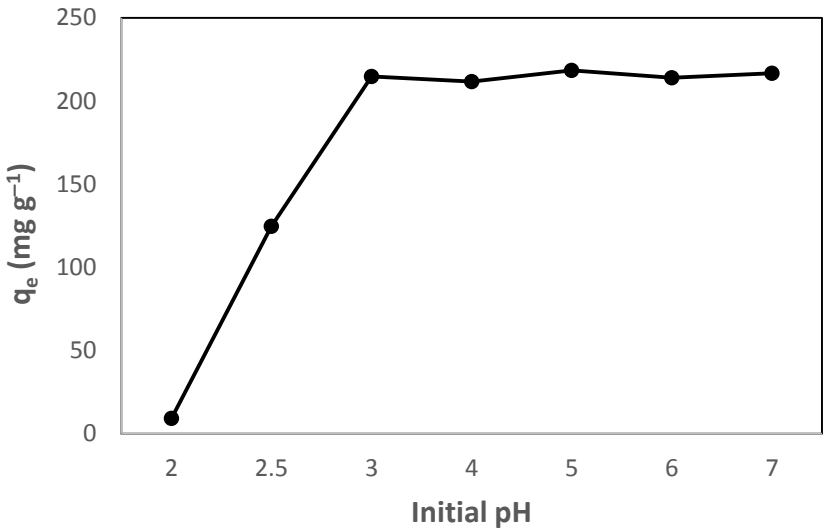


Figure 3.27 Effect of initial pH of $Cd^{2+}$ solution to cadmium adsorption capacity

# CHAPTER 4
# CONCLUSIONS AND SUGGESTIONS

## 4.1 Conclusions

Using simple precipitation method and citric acid as additive, magnetic calcium phosphate composites were successfully prepared in one-pot synthesis. Two types of calcium phosphates, including hydroxyapatite and amorphous were formed depending on the pH of the reaction mixture after adding citric acid. The synthesized composites possessed high $Cd^{2+}$ adsorption capacities, and the used absorbents could be separated easily from aqueous solution under an external magnetic field. Our results revealed that the high cadmium removal ability was obtained from the materials having low crystallinities. The ACP/$Fe_3O_4$/citric sample having Ca/P ratio of 1.5 exhibited the highest cadmium adsorption capacity. The adsorption kinetics and isotherms studied on the composite followed the pseudo-second-order and Langmuir model, respectively. Moreover, the cation exchange between $Ca^{2+}$ in calcium phosphates and $Cd^{2+}$ in the solution was found to be the adsorption mechanism. These findings could be beneficial to understand the adsorption behavior of the composites.

Having high cadmium removal capacities, simple preparation, low cost and convenient recovery, these composites could be very promising adsorbents for cadmium treatment in aqueous solution.



## 4.2 Suggestions for further research

To improve the application of these composites on cadmium removal, further research should investigate the reuse of the adsorbents. The study on using these materials to treat real waste water and the effects of interfering ions on the removal ability are also necessary.

# REFERENCES


[1] Bernhoft, R.A. Cadmium Toxicity and Treatment. The Scientific World Journal 2013 (2013): 7.

[2] Smičiklas, I.D., Milonjić, S.K., Pfendt, P., and Raičević, S. The point of zero charge and sorption of cadmium (II) and strontium (II) ions on synthetic hydroxyapatite. Separation and Purification Technology 18(3) (2000): 185-194.

[3] Purkayastha, D., Mishra, U., and Biswas, S. A comprehensive review on Cd(II) removal from aqueous solution. Journal of Water Process Engineering 2 (2014): 105-128.

[4] Ding, G.-J., Zhu, Y.-J., Qi, C., Sun, T.-W., Wu, J., and Chen, F. Amorphous calcium phosphate nanowires prepared using beta-glycerophosphate disodium salt as an organic phosphate source by a microwave-assisted hydrothermal method and adsorption of heavy metals in water treatment. RSC Advances 5(50) (2015): 40154-40162.

[5] Chen, S.B., Ma, Y.B., Chen, L., and Xian, K. Adsorption of aqueous $Cd^{2+}$, $Pb^{2+}$, $Cu^{2+}$ ions by nano-hydroxyapatite: Single- and multi-metal competitive adsorption study. Geochem. J. 44(3) (2010): 233-239.

[6] Corami, A., Mignardi, S., and Ferrini, V. Cadmium removal from single- and multi-metal (Cd + Pb + Zn + Cu) solutions by sorption on hydroxyapatite. Journal of Colloid and Interface Science 317(2) (2008): 402-408.

[7] Middelburg, J.J. and Comans, R.N.J. Sorption of cadmium on hydroxyapatite. Chemical Geology 90(1–2) (1991): 45-53.

[8] Mobasherpour, I., Salahi, E., and Pazouki, M. Removal of nickel (II) from aqueous solutions by using nano-crystalline calcium hydroxyapatite. Journal of Saudi Chemical Society 15(2) (2011): 105-112.

[9] Mobasherpour, I., Salahi, E., and Pazouki, M. Comparative of the removal of $Pb^{2+}$, $Cd^{2+}$ and $Ni^{2+}$ by nano crystallite hydroxyapatite from aqueous solutions: Adsorption isotherm study. Arabian Journal of Chemistry 5(4) (2012): 439-446.

[10] Sandrine, B., Ange, N., Didier, B.-A., Eric, C., and Patrick, S. Removal of aqueous lead ions by hydroxyapatites: Equilibria and kinetic processes. Journal of Hazardous Materials 139(3) (2007): 443-446.

[11] Sugiyama, S., et al. Heavy metal immobilization in aqueous solution using calcium phosphate and calcium hydrogen phosphates. Journal of Colloid and Interface Science 259(2) (2003): 408-410.

[12] Fernane, F., Boudia, S., and Saouli, H. Interactions between calcium phosphate and heavy metal ions in aqueous solution. MATEC Web of Conferences 5 (2013): 04034.

[13] Feng, Y., et al. Adsorption of Cd (II) and Zn (II) from aqueous solutions using magnetic hydroxyapatite nanoparticles as adsorbents. Chemical Engineering Journal 162(2) (2010): 487-494.

[14] Zhu, R., Yu, R., Yao, J., Mao, D., Xing, C., and Wang, D. Removal of $Cd^{2+}$ from aqueous solutions by hydroxyapatite. Catalysis Today 139(1–2) (2008): 94-99.

[15] Xu, Y., Schwartz, F.W., and Traina, S.J. Sorption of $Zn^{2+}$ and $Cd^{2+}$ on Hydroxyapatite Surfaces. Environmental Science & Technology 28(8) (1994): 1472-1480.

[16] Lu, X., et al. Hexagonal hydroxyapatite formation on $TiO_2$ nanotubes under urea modulation. CrystEngComm 13(11) (2011): 3741-3749.

[17] Smičiklas, I., Onjia, A., Raičević, S., Janaćković, Đ., and Mitrić, M. Factors influencing the removal of divalent cations by hydroxyapatite. Journal of Hazardous Materials 152(2) (2008): 876-884.

[18] Yasukawa, A., Yokoyama, T., Kandori, K., and Ishikawa, T. Reaction of calcium hydroxyapatite with $Cd^{2+}$ and $Pb^{2+}$ ions. Colloids and Surfaces A: Physicochemical and Engineering Aspects 299(1–3) (2007): 203-208.

[19] Ronghai Zhu, R.Y., Jianxi Yao, Dan Mao, Chaojian Xing, Dan Wang a,. Removal of $Cd^{2+}$ from aqueous solutions by hydroxyapatite. Catalysis Today 139 (2008): 94-99.

[20] K.S. Rao, M.M., S. Anand, P. Venkateswarlu. Review on cadmium removal from aqueous solutions. International Journal of Engineering, Science and Techonology 2 (2010): 81-103.

[21] Shahin Hydari, H.S., Mahboobeh Nabavinia, Mohammad reza Parvizi. A comparative investigation on removal performances of commercial activated carbon, chitosan biosorbent and chitosan/activated carbon composite for cadmium. Chemical Engineering Journal 193-194 (2012): 276-282.

[22] Nayak, A.K. Hydroxyapatite Synthesis Methodologies: An Overview. International Journal of ChemTech Research 2 (2010): 903-907.

[23] Somrani, S., Banu, M., Jemal, M., and Rey, C. Physico-chemical and thermochemical studies of the hydrolytic conversion of amorphous tricalcium phosphate into apatite. Journal of Solid State Chemistry 178(5) (2005): 1337-1348.

[24] Williams, G. and Sallis, J.D. Structure--activity relationship of inhibitors of hydroxyapatite formation. Biochemical Journal 184(1) (1979): 181-184.

[25] Du, L.-W., et al. Structure of Clusters and Formation of Amorphous Calcium Phosphate and Hydroxyapatite: From the Perspective of Coordination Chemistry. Crystal Growth & Design 13(7) (2013): 3103-3109.

[26] Sun, L., Chow, L.C., Frukhtbeyn, S.A., and Bonevich, J.E. Preparation and Properties of Nanoparticles of Calcium Phosphates With Various Ca/P Ratios. Journal of Research of the National Institute of Standards and Technology 115(4) (2010): 243-255.

[27] Combes, C. and Rey, C. Amorphous calcium phosphates: Synthesis, properties and uses in biomaterials. Acta Biomaterialia 6(9) (2010): 3362-3378.

[28] Ding, G.-J., Zhu, Y.-J., Qi, C., Lu, B.-Q., Wu, J., and Chen, F. Porous microspheres of amorphous calcium phosphate: Block copolymer templated microwave-assisted hydrothermal synthesis and application in drug delivery. Journal of Colloid and Interface Science 443 (2015): 72-79.

[29] Maciejewski, M., Brunner, T.J., Loher, S.F., Stark, W.J., and Baiker, A. Phase transitions in amorphous calcium phosphates with different Ca/P ratios. Thermochimica Acta 468(1–2) (2008): 75-80.

[30] Mekmene, O., Quillard, S., Rouillon, T., Bouler, J.-M., Piot, M., and Gaucheron, F. Effects of pH and Ca/P molar ratio on the quantity and crystalline structure

of calcium phosphates obtained from aqueous solutions. Dairy Science & Technology 89(3) (2009): 301-316.

[31] Stötzel, C., Müller, F.A., Reinert, F., Niederdraenk, F., Barralet, J.E., and Gbureck, U. Ion adsorption behaviour of hydroxyapatite with different crystallinities. Colloids and Surfaces B: Biointerfaces 74(1) (2009): 91-95.

[32] Zhuang, F., Tan, R., Shen, W., Zhang, X., Xu, W., and Song, W. Monodisperse magnetic hydroxyapatite/$Fe_3O_4$ microspheres for removal of lead(II) from aqueous solution. Journal of Alloys and Compounds 637 (2015): 531-537.

[33] Yang, H., Masse, S., Zhang, H., Hélary, C., Li, L., and Coradin, T. Surface reactivity of hydroxyapatite nanocoatings deposited on iron oxide magnetic spheres toward toxic metals. Journal of Colloid and Interface Science 417 (2014): 1-8.

[34] Foroughi, F., Hassanzadeh-Tabrizi, S.A., and Amighian, J. Microemulsion synthesis and magnetic properties of hydroxyapatite-encapsulated nano $CoFe_2O_4$. Journal of Magnetism and Magnetic Materials 382 (2015): 182-187.

[35] Suvokhiaw, S., Imyim, A., and Sukpirom, N. As(V) removal using a magnetic layered double hydroxide composite. Separation Science and Technology 51(18) (2016): 2948-2957.

[36] Iraj Kazeminezhad, S.A. Application of Magnetic Hydroxyapatite Nanoparticles for Removal of $Cd^{2+}$ from Aqueous Solutions. Journal of Environmental Studies 40(37-39) (2014).

[37] Rout, S.R., Behera, B., Maiti, T.K., and Mohapatra, S. Multifunctional magnetic calcium phosphate nanoparticles for targeted platin delivery. Dalton Transactions 41(35) (2012): 10777-10783.

[38] Hu, Y.Y., Rawal, A., and Schmidt-Rohr, K. Strongly bound citrate stabilizes the apatite nanocrystals in bone. Proceedings of the National Academy of Sciences of the United States of America 107(52) (2010): 22425-22429.

[39] Kakiage, M., Iwase, K., and Kobayashi, H. Effect of citric acid addition on disaggregation of crystalline hydroxyapatite nanoparticles under calcium-rich conditions. Materials Letters 156 (2015): 39-41.

[40] Rhee, S.-H. and Tanaka, J. Effect of citric acid on the nucleation of hydroxyapatite in a simulated body fluid. Biomaterials 20(22) (1999): 2155-2160.

[41] Sousa, M.E., et al. Stability and Relaxation Mechanisms of Citric Acid Coated Magnetite Nanoparticles for Magnetic Hyperthermia. The Journal of Physical Chemistry C 117(10) (2013): 5436-5445.

[42] Elham Cheraghipour, S.J., Ali Reza Mehdizadeh. Citrate capped superparamagnetic iron oxide nanoparticles used for hyperthermia therapy. J. Biomedical Science and Engineering 5 (2012): 715-719.

[43] Goodarzi, A., Sahoo, Y., Swihart, M.T., and Prasad, P.N. Aqueous Ferrofluid of Citric Acid Coated Magnetite Particles. MRS Proceedings 789 (2003).

[44] Goss, S., Prushko, J., and Bogner, R. Factors Affecting Calcium Precipitation During Neutralisation in a Simulated Intestinal Environment. Journal of Pharmaceutical Sciences 99(10): 4183-4191.

[45] Hu, Y.Y., Liu, X.P., Ma, X., Rawal, A., and Prozorov, T. Biomimetic Self-Assembling Copolymer–Hydroxyapatite Nanocomposites with the Nanocrystal Size Controlled by Citrate. in Chemistry of Materials. 2011, American Chemical Society. 2481-2490.

[46] Achelhi, K., Masse, S., Laurent, G., Saoiabi, A., Laghzizil, A., and Coradin, T. Role of carboxylate chelating agents on the chemical, structural and textural properties of hydroxyapatite. Dalton Transactions 39(44) (2010): 10644-10651.

[47] Saoiabi, S., Achelhi, K., Masse, S., Saoiabi, A., Laghzizil, A., and Coradin, T. Organo-apatites for lead removal from aqueous solutions: A comparison between carboxylic acid and aminophosphonate surface modification. Colloids and Surfaces A: Physicochemical and Engineering Aspects 419 (2013): 180-185.

[48] Hong, R.-Y., et al. Preparation and characterization of silica-coated $Fe_3O_4$ nanoparticles used as precursor of ferrofluids. Applied Surface Science 255(6) (2009): 3485-3492.

[49] Jantaratana, P., Noodam, J., and Sirisathitkul, C. Magnetic Hysteresis and Electrical Impedance Spectra of Hard Magnetic $SmCo_5$ and Soft Magnetic $Co_{30}Ag_{70}$ Composites. Rare Metal Materials and Engineering 42(1) (2013): 19-22.

[50] Sing, K.S.W.E., Douglas H. Haul, R. A. W. Moscou, L. Pierotti, Robert A. Rouquerol, Jean Siemieniewska, Teresa. Reporting physisorption data for gas/solid systems

with special reference to the determination of surface area and porosity. International Union of Pure and Applied Chemistry 57 (1985): 603—619.

[51] Martins, M.A., Santos, C., Almeida, M.M., and Costa, M.E.V. Hydroxyapatite micro- and nanoparticles: Nucleation and growth mechanisms in the presence of citrate species. Journal of Colloid and Interface Science 318(2) (2008): 210-216.

[52] Stachurski, Z.H. On Structure and Properties of Amorphous Materials. Materials 4(9) (2011): 1564.

[53] Cai, Y.Q., Storer, P., Kheifets, A.S., McCarthy, I.E., and Weigold, E. Dangling-bond surface states on an amorphous germanium surface as observed by (e,2e) spectroscopy. Surface Science 357 (1996): 427-431.

[54] Patsula, V., et al. Superparamagnetic $Fe_3O_4$ Nanoparticles: Synthesis by Thermal Decomposition of Iron(III) Glucuronate and Application in Magnetic Resonance Imaging. ACS Applied Materials & Interfaces 8(11) (2016): 7238-7247.

[55] Pan, J., et al. Magnetic molecularly imprinted polymers based on attapulgite/$Fe_3O_4$ particles for the selective recognition of 2,4-dichlorophenol. Chemical Engineering Journal 174(1) (2011): 68-75.

[56] Milonjić, S.K., Kopečni, M.M., and Ilić, Z.E. The point of zero charge and adsorption properties of natural magnetite. Journal of Radioanalytical Chemistry 78(1) (1983): 15-24.

[57] Wyrzykowski, D., Hebanowska, E., Nowak-Wiczk, G., Makowski, M., and Chmurzynski, L. Thermal behaviour of citric acid and isomeric aconitic acids. Journal of Thermal Analysis and Calorimetry 104(2) (2011): 731-735.

[58] Fehr, M., et al. Dangling bonds in amorphous silicon investigated by multifrequency EPR. Journal of Non-Crystalline Solids 358(17) (2012): 2067-2070.

[59] Freysoldt, C., Pfanner, G., and Neugebauer, J. The dangling-bond defect in amorphous silicon: Statistical random versus kinetically driven defect geometries. Journal of Non-Crystalline Solids 358(17) (2012): 2063-2066.

# APPENDIX

# VITA

Miss Trang Thuy Thuy Le Hoang was born on July 28th, 1991 in Dong Nai, Vietnam. She received her Bachelor Degree of Science in Chemistry, Ho Chi Minh City University of Science, Vietnam in 2013. She continued her study in program of Inorganic Chemistry, Faculty of Science, Chulalongkorn University in 2014 and completed in 2016.

Poster presentation "Synthesis of hydroxyapatite using citric acid as additive for removal of cadmium in aqueous solution", the 42nd Congress on Science and Technology of Thailand, November 29 – December 2, Central Plaza Ladprao, Bangkok, Thailand.

Her present address is CU iHouse, 268 Chulalongkorn Soi9, Charasmuang road, Wangmai, Pathumwan, Bangkok, Thailand.